

HYPER-DIFFERENTIAL SENSITIVITY ANALYSIS WITH RESPECT TO MODEL DISCREPANCY: CALIBRATION AND OPTIMAL SOLUTION UPDATING *

JOSEPH HART[†] AND BART VAN BLOEMEN WAANDERS[‡]

Abstract. Optimization constrained by computational models is common across science and engineering. However, in many cases a high-fidelity model of the system cannot be optimized due to its complexity and computational cost. Rather, a low(er)-fidelity model is constructed to enable intrusive and many query algorithms needed for large-scale optimization. As a result of the discrepancy between the high and low-fidelity models, the optimal solution determined using the low-fidelity model is frequently far from true optimality. In this article we introduce a novel approach which uses limited high-fidelity data to calibrate the model discrepancy in a Bayesian framework and propagate it through the optimization problem. The result provides both an improvement in the optimal solution and a characterization of uncertainty due to the limited accessibility of high-fidelity data. Our formulation exploits structure in the post-optimality sensitivity operator to ensure computational scalability. Numerical results demonstrate how an optimal solution computed using a low-fidelity model may be significantly improved with as little as one evaluation of a high-fidelity model.

Key words. Hyper-differential sensitivity analysis, post-optimality sensitivity analysis, PDE-constrained optimization, model discrepancy

AMS subject classifications. 65K10,65G99

1. Introduction. Optimization problems constrained by computational models are ubiquitous in science and engineering and have been the topic of extensive research. Nonetheless, optimization problems are only as useful as the models which constrain them, and in the case of large-scale science and engineering applications, the models are frequently flawed due to the complexity of the system being modeled. Errors arise from many sources such as incomplete knowledge of the system physics or a lack of computational resources to accurately simulate the model. Hence the use of such models in optimization algorithms mandate rigorous analysis of how modeling errors influence the optimal solution.

We use the terminology model form error (or model error) to describe errors in the mathematical form of the model, for instance, missing an operator in a differential equation or using a phenomenological model for an unclosed component in a system. The presence of model form error causes the solution predicted by the model to differ from reality. The difference between a model’s prediction and reality is referred to as the model discrepancy. This article focuses on how model discrepancy influences optimization problems, assuming that a high-fidelity data source is available to calibrate the discrepancy. We focus on problems where the high-fidelity data source is a computational model which may only be evaluated a small number of times. Computational models rarely predict reality perfectly, but in the scope of this article we consider a high-fidelity computational model as the “gold standard” for comparison.

In many applications, a high-fidelity model exists but cannot be instrumented for optimization due to its software complexity and computational cost. This is common in many production codes which are developed over many years by large teams with

*Submitted to the editors DATE.

[†]Scientific Machine Learning, Sandia National Laboratories, P.O. Box 5800, Albuquerque, NM 87123-1320 (joshart@sandia.gov).

[‡]Scientific Machine Learning, Sandia National Laboratories, P.O. Box 5800, Albuquerque, NM 87123-1320 (bartv@sandia.gov).

a goal toward achieving model fidelity rather than enabling optimization or other intrusive analysis approaches. In such cases, a low(er)-fidelity model is constructed to enable efficient optimization. We assume that an optimization problem has been solved using this low-fidelity model and pose the question: “How can a small number of evaluations from the high-fidelity model be used to improve the optimal solution?” This may be used in a variety of applications including, but not limited to, real-time optimization for system control, engineering design, geophysical monitoring and characterization, and system health monitoring. The low-fidelity model may arise from model order reduction methods or making assumptions on the physical process to yield simpler equations which are more easily simulated.

Common practice is to optimize the low-fidelity model and use limited evaluations of the high-fidelity model to validate the solution. This work goes a step further and seeks to use the high-fidelity data to improve the optimal solution. Given that the space of optimal solutions is large and the number of high-fidelity solves is small, it is critical that we also characterize uncertainty due to the data sparsity. Building on hyper-differential sensitivity analysis (HDSA) with respect to model discrepancy [22], we formulate a Bayesian inverse problem coupled with HDSA to update the optimal solution and characterize uncertainty in it. To position this work in the literature, we highlight three distinct research areas and note how our proposed approach is similar and different from each of them.

The first area is the model discrepancy literature which grew out of the seminal work of Kennedy and O’Hagan [29]. In it, an additive model discrepancy is calibrated alongside the model parameters in a Bayesian framework to account for uncertainty and correlations between the discrepancy and parameters. This was followed by many works which analyzed and extended their approach, [3, 11, 16, 26, 32, 33, 36]. We take inspiration from their work in both the choice of an additive discrepancy function and its Bayesian representation; however, we depart from this literature in a significant way by assuming that a high-fidelity model may be queried for different values of the optimization variables. In the calibration context, the model discrepancy is accessed through observed data with an implicit dependence on the calibration parameters which are not known. In contrast, we consider general optimization problems and assume knowledge of and an ability to control the parameter settings in the high-fidelity model evaluations. For this reason, we focus on optimal control and design problems; however, model calibration may still be considered from a different perspective than Kennedy and O’Hagan.

The second area is the multi-fidelity methods literature [37]. Motivated by a need to enable outer loop analysis such as optimization and uncertainty quantification, this literature seeks to develop algorithms which combine evaluations of high and low-fidelity models to achieve accuracy commensurate to the high-fidelity model at a lower computational cost. This has seen considerable interest in the context of accelerating Monte Carlo type analysis [17] for general uncertainty quantification applications as well as in the specific context of optimization under uncertainty [34, 35]. There has also been work to combine high and low-fidelity model evaluations within each iterate of a deterministic optimization algorithm [1, 12]. Similarly, we assume access to both a high and low-fidelity model; however, unlike the previous references we seek a framework where the optimization problem does not require access to the high-fidelity model. Further, our focus is on cases where the number of high-fidelity solves is significantly constrained and they must be performed offline. We cannot provide theoretical guarantees which multi-fidelity methods ensure through recourse on the high-fidelity model, but our framework is suited for many applications where multi-

fidelity optimization is infeasible due to the complexity of the high-fidelity model.

The third area is the post-optimality sensitivity analysis [8, 15] literature. Arising out of optimization, this line of research has focused on the sensitivity of optimization problems to parametric uncertainty. It was originally developed in the context of operations research and then extended to optimization constrained by partial differential equations (PDEs) [10, 18, 19]. Building on this, hyper-differential sensitivity analysis scaled post-optimality sensitivities to high-dimensions through a coupling of tools from PDE-constrained optimization and numerical linear algebra [21, 23, 24, 39, 41, 42]. These previous references considered parametric uncertainties, whereas recent work [22] has extended the framework to parameterizations of model discrepancy. Our foundation in [22] provides computationally advantageous expressions determine the sensitivity of PDE-constrained optimization problems with respect to model discrepancy. This article introduces a Bayesian formulation to calibrate the model discrepancy and efficiently propagate its posterior through the post-optimality sensitivity operator. This enables a systematic integration of prior knowledge, high-fidelity data, and low-fidelity optimization in a pragmatic way for large-scale applications.

In what follows, Section 2 introduces the optimization problem under consideration and reviews the model discrepancy sensitivities introduced in [22]. Section 3 presents the article’s contributions to formulate and solve the discrepancy calibration problem and propagate its posterior through the post-optimality sensitivity operator. The proposed algorithm is summarized and its computational cost is analyzed in Section 4. We show numerical results in Section 5 for an illustrative thermal control example and a more complex fluid flow example where the Stokes equation is used as a low-fidelity approximation of the Navier-Stokes equation. Using only one forward solve with the Navier-Stokes model, we are able to improve the quality of the Stokes optimal solution by two orders of magnitude in the objective function. We conclude in Section 6 with a forward looking perspective on how this research may impact a variety of science and engineering applications.

2. Background. This section provides the essential background to set up the contributions of the article.

2.1. Optimization formulation. Consider optimization problems of the form

$$(2.1) \quad \min_{z \in \mathcal{Z}} J(S(z), z)$$

where z denotes an optimization variable in the Hilbert space \mathcal{Z} , $S : \mathcal{Z} \rightarrow \mathcal{U}$ denotes the solution operator for a PDE (partial differential equation) $c(u, z) = 0$ with state variable u in a Hilbert space \mathcal{U} , and $J : \mathcal{U} \times \mathcal{Z} \rightarrow \mathbb{R}$ is the objective function. We allow for the possibility that \mathcal{Z} and \mathcal{U} are infinite dimensional. This formulation is applicable for many design, control, and inverse problems. For simplicity we will call z the “parameters” though its name varies depending upon the context.

The PDE-constrained optimization literature is vast. Noteworthy components include adjoint-based derivative computation, Krylov and Newton iterative solves, and parallel numerical linear algebra as critical to enable scalable computation. The reader may see [2, 4–7, 9, 20, 25, 27, 28, 30, 31, 43, 44] for additional details.

The high-fidelity PDE governing the system may be too complex and/or computationally intensive to optimize, so in practice we solve

$$(2.2) \quad \min_{z \in \mathcal{Z}} J(\tilde{S}(z), z)$$

where $\tilde{S} : \mathcal{Z} \rightarrow \mathcal{U}$ is the solution operator for a simpler model $\tilde{c}(u, z) = 0$. The solution of the low-fidelity optimization problem (2.2) is used to approximate the solution of the high-fidelity optimization problem (2.1). The goal of this article is to analyze how uncertainty in the discrepancy, $S(z) - \tilde{S}(z)$, may be modeled and propagated through (2.2) to improve the optimal solution and characterize uncertainty in it.

We focus on the problem arising after discretization. To this end, let $\{\phi_i\}_{i=1}^m$ and $\{\psi_j\}_{j=1}^n$ be bases for finite dimensional subspaces $\mathcal{U}_h \subset \mathcal{U}$ and $\mathcal{Z}_h \subset \mathcal{Z}$, respectively. These may, for instance, be finite element basis functions. Let $\mathbf{u} \in \mathbb{R}^m$ and $\mathbf{z} \in \mathbb{R}^n$ denote coordinates in basis representations and

$$(\mathbf{M}_u)_{i,j} = (\phi_i, \phi_j)_{\mathcal{U}} \quad \text{and} \quad (\mathbf{M}_z)_{i,j} = (\psi_i, \psi_j)_{\mathcal{Z}}$$

be mass matrices which define inner products in \mathcal{U}_h and \mathcal{Z}_h using the coordinate vectors. The objective J and solution operator \tilde{S} are discretized by $\mathbf{J} : \mathbb{R}^m \times \mathbb{R}^n \rightarrow \mathbb{R}$ and $\tilde{\mathbf{S}} : \mathbb{R}^n \rightarrow \mathbb{R}^m$ to arrive at a finite dimensional optimization problem.

2.2. Model discrepancy and post-optimality sensitivities. To propagate model discrepancy through the optimization problem, we build on [22] which defines a representation of the discrepancy as $\delta(\mathbf{z}, \boldsymbol{\theta}) \approx \mathbf{S}(\mathbf{z}) - \tilde{\mathbf{S}}(\mathbf{z})$, a function of \mathbf{z} parameterized by $\boldsymbol{\theta}$. We assume that $\delta(\mathbf{z}, \boldsymbol{\theta}_0) = \mathbf{0} \forall \mathbf{z}$ when evaluated at $\boldsymbol{\theta}_0 = \mathbf{0}$. Consider the parameterized optimization problem

$$(2.3) \quad \min_{\mathbf{z} \in \mathbb{R}^n} \hat{\mathbf{J}}(\mathbf{z}, \boldsymbol{\theta}) := \mathbf{J}(\tilde{\mathbf{S}}(\mathbf{z}) + \delta(\mathbf{z}, \boldsymbol{\theta}), \mathbf{z})$$

which we assume has a local minimum $\bar{\mathbf{z}} \in \mathbb{R}^n$ satisfying the first and second order optimality conditions when $\boldsymbol{\theta} = \boldsymbol{\theta}_0$, i.e. $\bar{\mathbf{z}} \in \mathbb{R}^n$ is the optimal solution when model discrepancy is ignored.

Applying the Implicit Function Theorem to the equation $\nabla_{\mathbf{z}} \hat{\mathbf{J}}(\bar{\mathbf{z}}, \boldsymbol{\theta}_0) = \mathbf{0}$, we consider an operator $\mathbf{F} : \mathcal{N}(\boldsymbol{\theta}_0) \rightarrow \mathcal{N}(\bar{\mathbf{z}})$, defined on neighborhoods of the local solution, such that $\mathbf{F}(\boldsymbol{\theta})$ is a stationary point of (2.3), i.e.

$$\nabla_{\mathbf{z}} \hat{\mathbf{J}}(\mathbf{F}(\boldsymbol{\theta}), \boldsymbol{\theta}) = \mathbf{0} \quad \forall \boldsymbol{\theta} \in \mathcal{N}(\boldsymbol{\theta}_0).$$

Assuming positive definiteness of the Hessian for all $(\mathbf{F}(\boldsymbol{\theta}), \boldsymbol{\theta})$, \mathbf{F} maps the model discrepancy to the optimal solution. The Jacobian of \mathbf{F} with respect to $\boldsymbol{\theta}$, i.e. the sensitivity of the optimal solution to the model discrepancy, is given by

$$(2.4) \quad \mathbf{F}'_{\boldsymbol{\theta}}(\mathbf{0}) = -\mathbf{H}^{-1} \mathbf{B} \in \mathbb{R}^{n \times p}$$

where $\mathbf{H} = \nabla_{\mathbf{z}, \mathbf{z}} \hat{\mathbf{J}}(\bar{\mathbf{z}}, \mathbf{0}) \in \mathbb{R}^{n \times n}$ is the Hessian of $\hat{\mathbf{J}}$ and $\mathbf{B} = \nabla_{\mathbf{z}, \boldsymbol{\theta}} \hat{\mathbf{J}}(\bar{\mathbf{z}}, \mathbf{0}) \in \mathbb{R}^{n \times p}$ is the Jacobian of $\nabla_{\mathbf{z}} \hat{\mathbf{J}}$ with respect to $\boldsymbol{\theta}$, with both evaluated at the nominal solution $(\bar{\mathbf{z}}, \mathbf{0})$. We interpret $\mathbf{F}'_{\boldsymbol{\theta}}(\mathbf{0})$ as a Newton step which updates the optimal solution $\bar{\mathbf{z}}$ when the model discrepancy is perturbed.

To parameterize the discrepancy δ , observe that the difference in solution operators $\mathbf{S}(\mathbf{z}) - \tilde{\mathbf{S}}(\mathbf{z})$ is, in general, a nonlinear function of \mathbf{z} . However, for post-optimality sensitivity analysis, it is sufficient to consider a discrepancy which is linear in \mathbf{z} . Following the derivation in [22], we consider a linear operator which inputs \mathbf{z} and outputs the discrepancy (an element of the state space). Starting from a general linear operator on function spaces, parameterizing the operator with $\boldsymbol{\theta}$, and transforming to the coordinate space, we define the model discrepancy $\delta : \mathbb{R}^m \times \mathbb{R}^p \rightarrow \mathbb{R}^m$ as

$$(2.5) \quad \delta(\mathbf{z}, \boldsymbol{\theta}) = \begin{pmatrix} \mathbf{I}_m & \mathbf{I}_m \otimes \mathbf{z}^T \mathbf{M}_z \end{pmatrix} \boldsymbol{\theta}$$

where $\boldsymbol{\theta}_0 = (\theta_{0,0}, \theta_{1,0}, \dots, \theta_{m,0})^T \in \mathbb{R}^m$, $\boldsymbol{\theta}_i = (\theta_{i,1}, \theta_{i,2}, \dots, \theta_{i,n})^T \in \mathbb{R}^n$, $i = 1, 2, \dots, m$, and $\boldsymbol{\theta} = (\boldsymbol{\theta}_0^T, \boldsymbol{\theta}_1^T, \dots, \boldsymbol{\theta}_m^T)^T \in \mathbb{R}^p$, $p = m(n+1)$, and $\mathbf{I}_m \in \mathbb{R}^{m \times m}$ is the identity matrix. Our ordering of $\boldsymbol{\theta}$'s components enables an efficient expression of $\boldsymbol{\delta}$ using the Kronecker product \otimes . We emphasize that $\boldsymbol{\theta} \in \mathbb{R}^p$ may be extremely high dimensional and our resulting analysis relies on representing all computation as Kronecker products to execute linear algebra in \mathbb{R}^m and \mathbb{R}^n rather than \mathbb{R}^p .

To simplify the analysis which follows we assume that $\nabla_{\mathbf{z}, \mathbf{u}} \mathbf{J} = 0$. This holds on a wide range of problems in practice where the objective is defined by a performance criteria (tracking type, data misfit, etc.) on the state plus a regularization on the parameters. Differentiating the objective function $\hat{\mathbf{J}}(\mathbf{z}, \boldsymbol{\theta})$, we write the resulting mixed-second derivative in a Kronecker form as

$$(2.6) \quad \mathbf{B} = \tilde{\mathbf{S}}_{\mathbf{z}}^T \nabla_{\mathbf{u}, \mathbf{u}} \mathbf{J} \left(\mathbf{I}_m \quad \mathbf{I}_m \otimes \bar{\mathbf{z}}^T \mathbf{M}_z \right) + \left(\mathbf{0} \quad \nabla_{\mathbf{u}} \mathbf{J} \otimes \mathbf{M}_z \right) \in \mathbb{R}^{n \times p}$$

where $\tilde{\mathbf{S}}_{\mathbf{z}}$, $\nabla_{\mathbf{u}} \mathbf{J}$, and $\nabla_{\mathbf{u}, \mathbf{u}} \mathbf{J}$ are evaluated at $(\bar{\mathbf{u}}, \bar{\mathbf{z}})$, $\bar{\mathbf{u}} = \tilde{\mathbf{S}}(\bar{\mathbf{z}})$. By expressing \mathbf{B} using Kronecker products, which arise from the Jacobians of $\boldsymbol{\delta}(\mathbf{z}, \boldsymbol{\theta})$, we compress the sensitivity computation into \mathbb{R}^m and \mathbb{R}^n , thus avoiding computation in \mathbb{R}^p .

3. Updating and quantifying uncertainty in the optimal solution. Assume that the low-fidelity optimization problem (2.2) has been solved to determine $\bar{\mathbf{z}}$, but in addition we have access to N forward solves of the high-fidelity model \mathbf{S} for different inputs $\{\mathbf{z}_\ell\}_{\ell=1}^N$. Let $\mathbf{y}_\ell = \mathbf{S}(\mathbf{z}_\ell) - \tilde{\mathbf{S}}(\mathbf{z}_\ell)$, $\ell = 1, 2, \dots, N$, denote the corresponding evaluations of the model discrepancy at these inputs. In practice, the number of evaluations N will be small since evaluating $\mathbf{S}(\mathbf{z}_\ell)$ is computationally costly. Our goal is to use these limited high-fidelity evaluations to: (i) improve the optimal solution $\bar{\mathbf{z}}$ without requiring model modifications or additional nonlinear solves, and (ii) to characterize uncertainty in the optimal solution. Figure 1 depicts our proposed approach. In this section, we detail our contributions to enable this workflow, which include:

- 1 Defining a prior distribution on $\boldsymbol{\theta}$ to reflect knowledge of the discrepancy.
- 2 Formulating and solving (in closed form) a Bayesian inverse problem using the data $\{\mathbf{z}_\ell, \mathbf{y}_\ell\}_{\ell=1}^N$ to determine a distribution for $\boldsymbol{\theta}$.
- 3 Computing posterior samples of discrepancy and propagating them through the sensitivity operator to compute a distribution on the optimal solution.

Due to the high dimensionality of the model discrepancy parameterization, $\boldsymbol{\theta} \in \mathbb{R}^p$, it is critical that we are able to efficiently sample from the posterior. We make judicious choices in the problem formulation and proceed through simplifications of the linear algebra to derive an algorithm which is scalable. In particular, the complexity of the algorithm will scale with N , the number of high-fidelity forward solves, which we assume to be small. Because high-fidelity solves are limited, the uncertainty quantification framework we propose is crucial.

3.1. Defining the prior. To facilitate computation we use a Gaussian prior for $\boldsymbol{\theta}$ with mean $\mathbf{0}$ and a covariance matrix which incorporates prior knowledge. Such priors are common in infinite dimensional Bayesian inverse problems. Since $\boldsymbol{\theta} \in \mathbb{R}^p$ does not have a physical interpretation, we focus on defining priors in \mathbb{R}^m and \mathbb{R}^n (the state and parameter spaces) so that a prior on $\boldsymbol{\theta}$ may be derived from them.

Let $\mathbf{L} \in \mathbb{R}^{m \times m}$ be a symmetric positive definite matrix which encodes the known physics of the discrepancy. This may embed assumptions about the smoothness of $\boldsymbol{\delta}$, its boundary conditions, or penalize deviations from known conservation properties. A common approach takes \mathbf{L} as the square of a Laplacian like elliptic differential

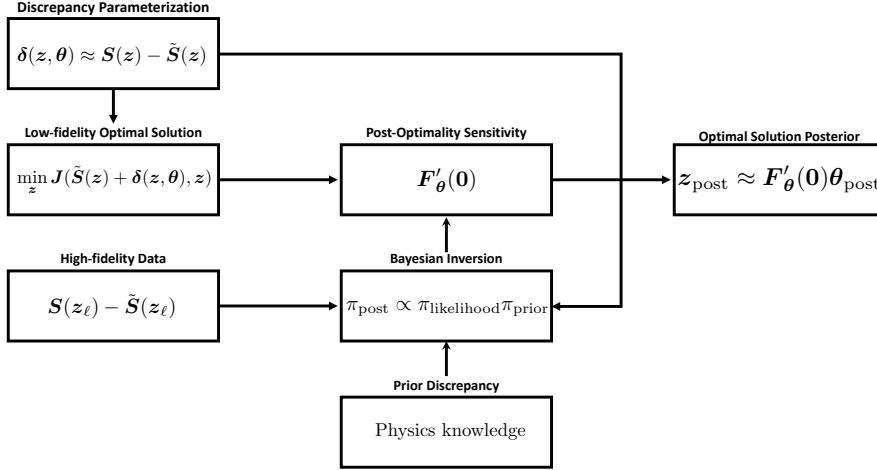


FIG. 1. *Diagram of the proposed analysis pipeline. We use π to denote probability distributions arising in the Bayesian inverse problem, and θ_{post} and \mathbf{z}_{post} to denote the random vectors distributed according to the discrepancy and optimal solution posteriors, respectively.*

operator (defined on the state space) so that \mathbf{L}^{-1} corresponds to the discretization of a well-defined prior covariance in the infinite dimensional state space [13, 38, 40].

The matrix \mathbf{L} imposes knowledge on the discrepancy independent of \mathbf{z} , it is only defined on \mathbb{R}^m rather than the product space \mathbb{R}^p . To impose prior knowledge about \mathbf{z} , we assume a Gaussian distribution with mean $\bar{\mathbf{z}}$ and covariance $\mathbf{\Gamma} \in \mathbb{R}^{n \times n}$ to model the space of possible parameters. This focuses our analysis around the nominal solution $\bar{\mathbf{z}}$ with deviation from it characterized by $\mathbf{\Gamma}$. There may be less prior information on \mathbf{z} since it is being determined through the optimization problem; however, $\mathbf{\Gamma}$ plays an important role defining characteristic length scales for \mathbf{z} .

Given \mathbf{L} and $\mathbf{\Gamma}$, along with the Kronecker structure of δ (2.5), we compute the expected value (with respect to \mathbf{z}) of the \mathbf{L} -weighted inner product of $\delta(\mathbf{z}, \theta)$ with itself and observe that it can be represented by the symmetric positive definite matrix

$$(3.1) \quad \mathbf{M}_\theta = \begin{pmatrix} \mathbf{L} & \mathbf{L} \otimes \bar{\mathbf{z}}^T \mathbf{M}_z \\ \mathbf{L} \otimes \mathbf{M}_z \bar{\mathbf{z}} & \mathbf{L} \otimes \mathbf{M}_z (\mathbf{\Gamma} + \bar{\mathbf{z}} \bar{\mathbf{z}}^T) \mathbf{M}_z \end{pmatrix} \in \mathbb{R}^{p \times p},$$

so that

$$\theta^T \mathbf{M}_\theta \theta = \mathbb{E}_{\mathbf{z}} [(\delta(\mathbf{z}, \theta), \delta(\mathbf{z}, \theta))_{\mathbf{L}}].$$

Hence \mathbf{M}_θ defines an inner product for θ to measure the size of the model discrepancy $\delta(\mathbf{z}, \theta)$ according to our prior knowledge imposed in \mathbf{L} and $\mathbf{\Gamma}$. This provides a mechanism to impose prior knowledge onto the state and parameter spaces and form the product space via the Kronecker structure of δ . Letting \mathbf{M}_θ^{-1} be the prior covariance for θ defines a prior that is rooted in established theory relating known physical properties to covariance matrices which may be efficiently manipulated [13, 38, 40].

As a building block for our subsequent analysis, note that we may decompose $\mathbf{M}_\theta = \mathbf{C}\mathbf{C}^T$ where

$$(3.2) \quad \mathbf{C} = \begin{pmatrix} \mathbf{L}^{\frac{1}{2}} & \mathbf{0} \\ \mathbf{L}^{\frac{1}{2}} \otimes \mathbf{M}_z \bar{\mathbf{z}} & \mathbf{L}^{\frac{1}{2}} \otimes \mathbf{M}_z \mathbf{\Gamma}^{\frac{1}{2}} \end{pmatrix}$$

and that

$$(3.3) \quad \mathbf{C}^{-1} = \begin{pmatrix} \mathbf{L}^{-\frac{1}{2}} & \mathbf{0} \\ \mathbf{L}^{-\frac{1}{2}} \otimes \left(-\mathbf{\Gamma}^{-\frac{1}{2}} \bar{\mathbf{z}}\right) & \mathbf{L}^{-\frac{1}{2}} \otimes \mathbf{\Gamma}^{-\frac{1}{2}} \mathbf{M}_z^{-1} \end{pmatrix}.$$

This factorization plays an important role enabling efficient manipulation and sampling of the posterior discrepancy distribution.

3.2. Bayesian inverse problem. We formulate a Bayesian inverse problem to estimate $\boldsymbol{\delta}$ using the data pairs $\{\mathbf{z}_\ell, \mathbf{y}_\ell\}_{\ell=1}^N$. To facilitate the analysis which follows we require:

ASSUMPTION 1. $\{\mathbf{z}_\ell\}_{\ell=1}^N$ is a linearly independent set of vectors in \mathbb{R}^n .

This is usually satisfied in practice as one explores the model space in different directions since the number of model evaluations N is small relative to the dimension of \mathbf{z} . For notational simplicity, we define

$$(3.4) \quad \mathbf{A}_\ell = \begin{pmatrix} \mathbf{I}_m & \mathbf{I}_m \otimes \mathbf{z}_\ell^T \mathbf{M}_z \end{pmatrix} \in \mathbb{R}^{m \times p}, \quad \ell = 1, 2, \dots, N,$$

so that $\boldsymbol{\delta}(\mathbf{z}_\ell, \boldsymbol{\theta}) = \mathbf{A}_\ell \boldsymbol{\theta}$, and the concatenation of these matrices

$$\mathbf{A} = \begin{pmatrix} \mathbf{A}_1 \\ \mathbf{A}_2 \\ \vdots \\ \mathbf{A}_N \end{pmatrix} \in \mathbb{R}^{mN \times p}$$

so that $\mathbf{A}\boldsymbol{\theta} \in \mathbb{R}^{mN}$ corresponds to the evaluation of $\boldsymbol{\delta}(\mathbf{z}, \boldsymbol{\theta})$ for all of the input data. In an analogous fashion, let $\mathbf{b} \in \mathbb{R}^{mN}$ be defined by stacking \mathbf{y}_ℓ , $\ell = 1, 2, \dots, N$, into a vector. Then we seek $\mathbf{A}\boldsymbol{\theta} \approx \mathbf{b}$.

To enable a closed form expression for the posterior we consider an additive Gaussian noise model with mean $\mathbf{0}$ and covariance $\alpha \mathbf{I}$, where $\alpha > 0$ is specified by the user. Typically the noise covariance in a Bayesian inverse problem is defined using knowledge of the data collection process. In cases where data is collected from simulation we do not have a clear definition of noise. Rather, we remember that $\boldsymbol{\delta}$ is defined as a linear function of \mathbf{z} , which is an approximation since $\mathbf{S}(\mathbf{z}) - \tilde{\mathbf{S}}(\mathbf{z})$ is, in general, a nonlinear function. Hence the noise may be interpreted as the approximation error due to the linearization of the discrepancy. Nonetheless, one can show that the range space of \mathbf{A} equals \mathbb{R}^{mN} , and hence there exists infinitely many $\boldsymbol{\theta} \in \mathbb{R}^p$ such that $\mathbf{A}\boldsymbol{\theta} = \mathbf{b}$. The user's choice of α dictates the weight given to the data misfit relative to the prior. Taking a small α will drive the inverse problem toward interpolation with little regard for the prior. We will demonstrate that the user may experiment with different α 's at a modest computational cost.

Given our formulation with Gaussian prior and noise models, and the linearity of $\boldsymbol{\delta}(\mathbf{z}, \boldsymbol{\theta})$ as a function of \mathbf{z} , the posterior is Gaussian with a (unnormalized) negative log probability density function

$$(3.5) \quad \frac{1}{2\alpha} (\mathbf{A}\boldsymbol{\theta} - \mathbf{b})^T (\mathbf{A}\boldsymbol{\theta} - \mathbf{b}) + \frac{1}{2} \boldsymbol{\theta}^T \mathbf{M}_\theta \boldsymbol{\theta}.$$

The posterior mean and covariance is given by

$$(3.6) \quad \bar{\boldsymbol{\theta}} = \frac{1}{\alpha} \boldsymbol{\Sigma} \mathbf{A}^T \mathbf{b} \quad \text{and} \quad \boldsymbol{\Sigma} = \left(\mathbf{M}_\theta + \frac{1}{\alpha} \mathbf{A}^T \mathbf{A} \right)^{-1}.$$

Samples from a Gaussian distribution may be generated by multiplying a factor of the covariance matrix with a standard normal random vector, and adding the mean. In what follows, we derive explicit and computationally efficient expressions for $\bar{\boldsymbol{\theta}}$ and a factorization of $\boldsymbol{\Sigma}$ to facilitate sampling.

3.3. Expressions for posterior sampling. We introduce a series of matrices and their factorizations to enable analysis of the posterior. Some of these expressions will not be computed but rather are intermediate steps toward our resulting algorithm. The computational requirements are made clear in Section 4 while this section presents the derivations from first principles. Emphasis is given to preserving the Kronecker product structure throughout our analysis so that computation in \mathbb{R}^p is never needed.

To aid the reader, we outline the derivation of posterior quantities and use section heading corresponding to the outline. The steps involved are:

1. Factorizing \mathbf{A} (to rewrite $\boldsymbol{\Sigma}^{-1}$ using a \mathbf{M}_θ orthogonal basis)
2. Inverting $\boldsymbol{\Sigma}^{-1}$ (by exploiting orthogonality to invert a sum)
3. Factorizing $\boldsymbol{\Sigma}$ (by determining an eigenvalue decomposition)
4. Computing posterior samples (by analytic matrix-vector multiplication)

Factorizing \mathbf{A} . To rewrite the inverse posterior covariance, $\mathbf{M}_\theta + \frac{1}{\alpha} \mathbf{A}^T \mathbf{A}$, in a form amenable for inversion, we decompose \mathbf{A} in a specially chosen inner product. In particular, the generalized singular value decomposition (GSVD) of \mathbf{A} with the \mathbf{M}_θ weighted inner product on the column space is given by $\mathbf{A} = \boldsymbol{\Xi} \boldsymbol{\Phi} \boldsymbol{\Psi}^T \mathbf{M}_\theta$, where $\boldsymbol{\Phi}$ is the diagonal matrix of singular values, and $\boldsymbol{\Xi}$ and $\boldsymbol{\Psi}$ are matrices containing the singular vectors which satisfy $\boldsymbol{\Xi}^T \boldsymbol{\Xi} = \mathbf{I}$ and $\boldsymbol{\Psi}^T \mathbf{M}_\theta \boldsymbol{\Psi} = \mathbf{I}$. To determine the singular vectors, notice that $\mathbf{A} \mathbf{M}_\theta^{-1} \mathbf{A}^T = \boldsymbol{\Xi} \boldsymbol{\Phi}^2 \boldsymbol{\Xi}^T$. Using the expressions (3.4) for \mathbf{A} and (3.3) for $\mathbf{M}_\theta^{-1} = \mathbf{C}^{-T} \mathbf{C}^{-1}$, we have

$$\mathbf{A} \mathbf{M}_\theta^{-1} \mathbf{A}^T = \mathbf{G} \otimes \mathbf{L}^{-1}$$

where

$$\mathbf{G} = \mathbf{e} \mathbf{e}^T + (\mathbf{Z} - \bar{\mathbf{z}} \mathbf{e}^T)^T \boldsymbol{\Gamma}^{-1} (\mathbf{Z} - \bar{\mathbf{z}} \mathbf{e}^T) \in \mathbb{R}^{N \times N},$$

where $\mathbf{Z} = (\mathbf{z}_1 \ \mathbf{z}_2 \ \dots \ \mathbf{z}_N)$ is the matrix of parameter data and $\mathbf{e} \in \mathbb{R}^N$ is the vector of ones. Hence the left singular vectors $\boldsymbol{\Xi}$ correspond to the eigenvectors of $\mathbf{G} \otimes \mathbf{L}^{-1}$ and the squared singular values $\boldsymbol{\Phi}^2$ correspond to the eigenvalues.

Letting $(\mathbf{g}_i, \lambda_i)$ and (\mathbf{l}_j, ρ_j) denote the eigenvectors and eigenvalues of \mathbf{G} and \mathbf{L} , respectively, and recalling properties of the eigenvalue decomposition of a Kronecker product, we observe that the squared generalized singular values of \mathbf{A} are given by $\frac{\lambda_i}{\rho_j}$ and are associated with the left singular vectors $\boldsymbol{\xi}_{i,j} = \mathbf{g}_i \otimes \mathbf{l}_j$. Rewriting the GSVD to solve for $\boldsymbol{\Psi}$, we see that the right singular vector associated with $\boldsymbol{\xi}_{i,j}$ is given by

$$(3.7) \quad \boldsymbol{\psi}_{i,j} = \frac{1}{\sqrt{\lambda_i \rho_j}} \begin{pmatrix} s_i \mathbf{l}_j \\ \mathbf{l}_j \otimes \mathbf{M}_z^{-1} \boldsymbol{\Gamma}^{-1} \mathbf{w}_i \end{pmatrix}, \quad i = 1, 2, \dots, N, j = 1, 2, \dots, m,$$

where

$$(3.8) \quad \mathbf{w}_i = \mathbf{Z} \mathbf{g}_i - (\mathbf{e}^T \mathbf{g}_i) \bar{\mathbf{z}} \quad \text{and} \quad s_i = (\mathbf{e}^T \mathbf{g}_i) - \mathbf{w}_i^T \boldsymbol{\Gamma}^{-1} \bar{\mathbf{z}}.$$

Given this decomposition of \mathbf{A} and our previously noted decomposition $\mathbf{M}_\theta = \mathbf{C} \mathbf{C}^T$, we express $\boldsymbol{\Sigma}^{-1}$ as

$$(3.9) \quad \boldsymbol{\Sigma}^{-1} = \frac{1}{\alpha} \mathbf{C} \mathbf{X} \mathbf{C}^T$$

where

$$(3.10) \quad \mathbf{X} = \alpha \mathbf{I} + \mathbf{C}^T \boldsymbol{\Psi} \boldsymbol{\Phi}^2 \boldsymbol{\Psi}^T \mathbf{C}.$$

Inverting $\boldsymbol{\Sigma}^{-1}$. This factorization of $\boldsymbol{\Sigma}^{-1}$ implies that $\boldsymbol{\Sigma} = \alpha \mathbf{C}^{-T} \mathbf{X}^{-1} \mathbf{C}^{-1}$. The benefit of our developments is that \mathbf{X} can be easily manipulated since it is a composition of diagonal and orthogonal matrices. Applying the Sherman-Morrison-Woodbury formula to (3.10), we have

$$\mathbf{X}^{-1} = \frac{1}{\alpha} (\mathbf{I} - \mathbf{C}^T \boldsymbol{\Psi} \mathbf{D} \boldsymbol{\Psi}^T \mathbf{C})$$

where $\mathbf{D} \in \mathbb{R}^{mN \times mN}$ is a diagonal matrix whose entries are given by $\frac{\lambda_i}{\lambda_i + \alpha \rho_j}$. Algebraic simplifications yield

$$(3.11) \quad \boldsymbol{\Sigma} = \mathbf{M}_\theta^{-1} - \boldsymbol{\Psi} \mathbf{D} \boldsymbol{\Psi}^T.$$

The posterior covariance may be interpreted as the prior covariance \mathbf{M}_θ^{-1} with its uncertainty reduced in the directions of the columns of $\boldsymbol{\Psi}$ (3.7) with weight $\frac{\lambda_i}{\lambda_i + \alpha \rho_j}$, a combination of the eigenvalues from \mathbf{L} and \mathbf{G} , along with the noise covariance α .

Factorizing $\boldsymbol{\Sigma}$. The expression (3.11) provides an interpretation of the posterior covariance and a way to compute the posterior mean $\bar{\boldsymbol{\theta}} = \frac{1}{\alpha} \boldsymbol{\Sigma} \mathbf{A}^T \mathbf{b}$. However, posterior sampling require a factorization of $\boldsymbol{\Sigma}$ which is not easily attained from (3.11). In pursuit of a factorization, we compute the eigenvalue decomposition of \mathbf{X} .

Notice that $(\mathbf{C}^T \boldsymbol{\Psi})^T (\mathbf{C}^T \boldsymbol{\Psi}) = \boldsymbol{\Psi}^T \mathbf{M}_\theta \boldsymbol{\Psi} = \mathbf{I}$, and hence the columns of $\mathbf{C}^T \boldsymbol{\Psi}$ are orthonormal in the Euclidean inner product. This implies that $\mathbf{C}^T \boldsymbol{\psi}_{i,j}$ is an eigenvector of \mathbf{X} with eigenvalue $\alpha + \frac{\lambda_i}{\rho_j}$. By multiplication using (3.2) and (3.7), we express these eigenvectors as

$$(3.12) \quad \mathbf{C}^T \boldsymbol{\psi}_{i,j} = \frac{1}{\sqrt{\lambda_i}} \begin{pmatrix} (\mathbf{e}^T \mathbf{g}_i) \mathbf{l}_j \\ \mathbf{l}_j \otimes \boldsymbol{\Gamma}^{-\frac{1}{2}} \mathbf{w}_i \end{pmatrix}.$$

This gives a total of mN eigenpairs of $\mathbf{X} \in \mathbb{R}^{p \times p}$. There are $p - mN = m(n - N + 1)$ additional eigenpairs of \mathbf{X} have the repeated eigenvalue α and eigenvectors from a set of orthonormal vectors that are orthogonal to the columns of $\mathbf{C}^T \boldsymbol{\Psi} \in \mathbb{R}^{p \times mN}$. To determine these remaining eigenpairs we suppose:

ASSUMPTION 2. $\mathbf{z}_1 = \bar{\mathbf{z}}$.

In words, we require that data is collected at the nominal optimal solution $\bar{\mathbf{z}}$, a reasonable assumption given that our goal is to use high-fidelity forward solves to improve it. Recalling (3.8) and using $\mathbf{z}_1 = \bar{\mathbf{z}}$, we observe that $\text{span}\{\mathbf{w}_i\}_{i=1}^N = \text{span}\{\mathbf{z}_\ell - \bar{\mathbf{z}}\}_{\ell=2}^N$ and let $\{\tilde{\mathbf{z}}_1, \tilde{\mathbf{z}}_2, \dots, \tilde{\mathbf{z}}_{n-N+1}\}$ in \mathbb{R}^n be an orthonormal set of vectors which are orthogonal to $\{\boldsymbol{\Gamma}^{-\frac{1}{2}}(\mathbf{z}_\ell - \bar{\mathbf{z}})\}_{\ell=2}^N$. Then remaining eigenvectors of \mathbf{X} are given by

$$(3.13) \quad \begin{pmatrix} \mathbf{0} \\ \mathbf{l}_j \otimes \tilde{\mathbf{z}}_k \end{pmatrix} \quad j = 1, 2, \dots, m, \quad k = 1, 2, \dots, n - N + 1.$$

Collecting this set of p eigenvectors (the union of (3.12) and (3.13)) in a orthogonal matrix \mathbf{Q} and the corresponding eigenvalues into a diagonal matrix $\boldsymbol{\Upsilon}$, the eigenvalue decomposition is given by

$$\mathbf{X} = \mathbf{Q} \boldsymbol{\Upsilon} \mathbf{Q}^T.$$

Hence, recalling (3.9), we decompose the covariance matrix as

$$(3.14) \quad \Sigma = \alpha \mathbf{C}^{-T} \mathbf{X}^{-1} \mathbf{C}^{-1} = \mathbf{T} \mathbf{T}^T$$

where

$$(3.15) \quad \mathbf{T} = \sqrt{\alpha} \mathbf{C}^{-T} \mathbf{Q} \Upsilon^{-\frac{1}{2}}.$$

The expression (3.15) facilitates efficient sampling, as we show below. Note that \mathbf{T} depends on $\{\tilde{\mathbf{z}}_1, \tilde{\mathbf{z}}_2, \dots, \tilde{\mathbf{z}}_{n-N+1}\}$, which is difficult to compute if n is large. However, as shown below, existence of the vectors $\{\tilde{\mathbf{z}}_1, \tilde{\mathbf{z}}_2, \dots, \tilde{\mathbf{z}}_{n-N+1}\}$ enables further derivations which culminate in expressions that do not require their explicit computation.

Computing posterior samples. Given the expressions (3.11) and (3.14), we write the posterior samples in terms of linear solves \mathbb{R}^m and \mathbb{R}^n . Our analysis thus far involves summing over all eigenpairs of \mathbf{L} , which poses computational challenges since the size of \mathbf{L} scales with the mesh resolution of the state. Rather, we will compute matrix-vector products and write the resulting vectors in terms of linear solves with \mathbf{L} rather than sums over its eigenpairs.

Using (3.6), (3.11) and (3.4), the posterior mean is given by

$$\bar{\theta} = \frac{1}{\alpha} \sum_{\ell=1}^N \left[\left(\mathbf{u}_\ell \otimes \mathbf{M}_z^{-1} \Gamma^{-1} (\mathbf{z}_\ell - \bar{\mathbf{z}}) \right) - \sum_{i=1}^N b_{i,\ell} \left(\mathbf{u}_{i,\ell} \otimes \mathbf{M}_z^{-1} \Gamma^{-1} \mathbf{w}_i \right) \right]$$

with constants

$$a_\ell = 1 - \bar{\mathbf{z}}^T \Gamma^{-1} (\mathbf{z}_\ell - \bar{\mathbf{z}}) \quad \text{and} \quad b_{i,\ell} = (\mathbf{z}_\ell - \bar{\mathbf{z}})^T \Gamma^{-1} \mathbf{Z} \mathbf{g}_i + (\mathbf{e}^T \mathbf{g}_i) a_\ell$$

and vectors

$$\mathbf{u}_\ell = \mathbf{L}^{-1} \mathbf{y}_\ell \quad \text{and} \quad \mathbf{u}_{i,\ell} = (\alpha \mathbf{L} + \lambda_i \mathbf{I})^{-1} \mathbf{u}_\ell.$$

We observe that it depends on linear solves¹ involving \mathbf{L} , Γ , and \mathbf{M}_z where the right hand sides arise from the data $\{\mathbf{z}_\ell, \mathbf{y}_\ell\}_{\ell=1}^N$. The posterior mean may be interpreted as a linear combination of the discrepancy data preconditioned by the prior with weights coming from the noise covariance α and the eigenvalues λ_i from the $\{\mathbf{z}_\ell\}_{\ell=1}^N$ data informed matrix \mathbf{G} .

To quantify uncertainty, we seek samples from the posterior distribution which take the form $\bar{\theta} + \mathbf{T} \omega$, where $\omega \sim \mathcal{N}(\mathbf{0}, \mathbf{I}_p)$ follows a standard normal distribution in \mathbb{R}^p . A direct calculation of $\mathbf{T} \omega$ poses problems as we cannot write the product in terms of linear solves with \mathbf{L} since the factorization $\Sigma = \mathbf{T} \mathbf{T}^T$ does not preserve the eigendecomposition of \mathbf{L} . To circumvent this, recall that Gaussian random vectors are invariant under orthogonal transformations. We introduce the orthogonal matrix $(\mathbf{I}_{n+1} \otimes \mathbf{V}^L)^T \in \mathbb{R}^{p \times p}$, where $\mathbf{V}^L \in \mathbb{R}^{m \times m}$ is the matrix whose columns are eigenvectors of \mathbf{L} . Then we sample $\omega = (\mathbf{I}_{n+1} \otimes \mathbf{V}^L)^T \nu$, where $\nu \in \mathcal{N}(\mathbf{0}, \mathbf{I}_p)$. With this transformation, we use (3.15) to compute posterior samples as

$$\mathbf{T} \omega = \mathbf{T} (\mathbf{I}_{n+1} \otimes \mathbf{V}^L)^T \nu = \hat{\theta} + \tilde{\theta}$$

¹In Section 5, we demonstrate how to efficiently invert \mathbf{L} and $(\alpha \mathbf{L} + \lambda_i \mathbf{I})$ using a generalized singular value decomposition when \mathbf{L} is defined as the square of an elliptic operator.

where

$$\hat{\boldsymbol{\theta}} = \sqrt{\alpha} \sum_{i=1}^N \frac{1}{\sqrt{\lambda_i}} \left(\hat{\mathbf{u}}_i \otimes \mathbf{M}_{\mathbf{z}}^{-1} \boldsymbol{\Gamma}^{-1} \mathbf{w}_i \right) \quad \text{and} \quad \tilde{\boldsymbol{\theta}} = \sum_{k=1}^{n-N+1} \begin{pmatrix} \tilde{s}_k \tilde{\mathbf{u}}_k \\ \tilde{\mathbf{u}}_k \otimes \tilde{\mathbf{w}}_k \end{pmatrix}$$

with

$$\begin{aligned} \hat{\mathbf{u}}_i &= (\alpha \mathbf{L} + \lambda_i \mathbf{I})^{-\frac{1}{2}} \boldsymbol{\nu}_i & \tilde{s}_k &= -\bar{\mathbf{z}}^T \boldsymbol{\Gamma}^{-\frac{1}{2}} \tilde{\mathbf{z}}_k \\ \tilde{\mathbf{u}}_k &= \mathbf{L}^{-\frac{1}{2}} \boldsymbol{\nu}_{N+k} & \tilde{\mathbf{w}}_k &= \mathbf{M}_{\mathbf{z}}^{-1} \boldsymbol{\Gamma}^{-\frac{1}{2}} \tilde{\mathbf{z}}_k \end{aligned}$$

and $\boldsymbol{\nu} = (\boldsymbol{\nu}_1^T, \boldsymbol{\nu}_2^T, \dots, \boldsymbol{\nu}_{n+1}^T)^T$, where $\boldsymbol{\nu}_i \in \mathbb{R}^m$, $i = 1, 2, \dots, n+1$. As in the expression for the mean $\bar{\boldsymbol{\theta}}$, the sample's components $\hat{\boldsymbol{\theta}}$ and $\tilde{\boldsymbol{\theta}}$ are written in terms of linear solvers with \mathbf{L} rather than its eigenpairs. This is made possible because of our formulation to apply \mathbf{T} to the vector $(\mathbf{I}_{n+1} \otimes \mathbf{V}^L)^T \boldsymbol{\nu}$ allows manipulation of the eigenvectors.

Combining these results, posterior samples for $\boldsymbol{\theta}$ may be decomposed as

$$\bar{\boldsymbol{\theta}} + \hat{\boldsymbol{\theta}} + \tilde{\boldsymbol{\theta}}$$

where $\bar{\boldsymbol{\theta}}$ is the mean (a deterministic quantity), $\hat{\boldsymbol{\theta}}$ is a random vector modeling uncertainty in directions informed that the data, and $\tilde{\boldsymbol{\theta}}$ is a random vector modeling uncertainty in directions which are not informed by the data.

3.4. Posterior model discrepancy. Substituting the expressions for $\bar{\boldsymbol{\theta}}$, $\hat{\boldsymbol{\theta}}$, and $\tilde{\boldsymbol{\theta}}$ into (2.5), samples of the posterior model discrepancy are given by

$$(3.16) \quad \delta(\mathbf{z}, \bar{\boldsymbol{\theta}} + \hat{\boldsymbol{\theta}} + \tilde{\boldsymbol{\theta}}) = \bar{\delta}(\mathbf{z}) + \hat{\delta}(\mathbf{z}) + \tilde{\delta}(\mathbf{z})$$

where

$$(3.17) \quad \begin{aligned} \bar{\delta}(\mathbf{z}) &= \frac{1}{\alpha} \sum_{\ell=1}^N (1 + (\mathbf{z}_\ell - \bar{\mathbf{z}})^T \boldsymbol{\Gamma}^{-1} (\mathbf{z} - \bar{\mathbf{z}})) \mathbf{u}_\ell \\ &\quad - \frac{1}{\alpha} \sum_{\ell=1}^N \sum_{i=1}^N b_{i,\ell} (e^T \mathbf{g}_i + \mathbf{w}_i^T \boldsymbol{\Gamma}^{-1} (\mathbf{z} - \bar{\mathbf{z}})) \mathbf{u}_{i,\ell} \end{aligned}$$

corresponds to evaluating the mean model discrepancy,

$$(3.18) \quad \hat{\delta}(\mathbf{z}) = \sqrt{\alpha} \sum_{i=1}^N \frac{1}{\sqrt{\lambda_i}} (e^T \mathbf{g}_i + \mathbf{w}_i^T \boldsymbol{\Gamma}^{-1} (\mathbf{z} - \bar{\mathbf{z}})) \hat{\mathbf{u}}_i$$

represents discrepancy uncertainty in the directions defined by the data $\{\mathbf{z}_\ell\}_{\ell=1}^N$, and

$$\tilde{\delta}(\mathbf{z}) = \sum_{k=1}^{n-N+1} \left(\tilde{\mathbf{z}}_k^T \boldsymbol{\Gamma}^{-\frac{1}{2}} (\mathbf{z} - \bar{\mathbf{z}}) \right) \tilde{\mathbf{u}}_k$$

represents discrepancy uncertainty in directions informed exclusively by the prior.

Observe that $\tilde{\delta}(\mathbf{z}_\ell) = 0$, $\ell = 1, 2, \dots, N$, i.e. $\tilde{\delta}$ vanishes in data informed directions, since $\{\tilde{\mathbf{z}}_k\}_{k=1}^{n-N+1}$ are orthogonal to $\{\boldsymbol{\Gamma}^{-\frac{1}{2}} (\mathbf{z}_\ell - \bar{\mathbf{z}})\}_{\ell=1}^N$. Further, observe that

$$\bar{\delta}(\bar{\mathbf{z}} + \boldsymbol{\Gamma}^{\frac{1}{2}} \tilde{\mathbf{z}}_k) = \bar{\delta}(\bar{\mathbf{z}}) \quad \text{and} \quad \hat{\delta}(\bar{\mathbf{z}} + \boldsymbol{\Gamma}^{\frac{1}{2}} \tilde{\mathbf{z}}_k) = \hat{\delta}(\bar{\mathbf{z}}) \quad k = 1, 2, \dots, n - N + 1$$

i.e. they do not vary in directions orthogonal to the data. In addition, notice that as $\alpha \rightarrow 0$, $\bar{\delta}(\mathbf{z})$ seeks to interpolate the observed data since $\bar{\boldsymbol{\theta}}$ is a minimizer of (3.5), while $\hat{\delta}(\mathbf{z}) \rightarrow 0$ as $\alpha \rightarrow 0$, indicating full confidence in the data interpolation. $\tilde{\delta}(\mathbf{z})$ does not depend on α since it acts in directions orthogonal to the data and thus captures uncertainty from the prior in directions which are not informed by data.

3.5. Applying the sensitivity operator to posterior samples. To characterize uncertainty in the solution of the optimization problem, we propagate posterior samples $\bar{\boldsymbol{\theta}} + \hat{\boldsymbol{\theta}} + \tilde{\boldsymbol{\theta}}$ through the post-optimality sensitivity operator $\mathbf{F}'_{\boldsymbol{\theta}}(\mathbf{0})$. Given the Kronecker product structure previously highlighted, we compute the action of \mathbf{B} on samples and then apply $-\mathbf{H}^{-1}$ to the resulting vectors. Observe that

$$(3.19) \quad \begin{aligned} \mathbf{B}\bar{\boldsymbol{\theta}} &= \frac{1}{\alpha} \tilde{\mathbf{S}}_z^T \nabla_{\mathbf{u}, \mathbf{u}} \mathbf{J} \left[\sum_{\ell=1}^N \left(\mathbf{u}_{\ell} - \sum_{i=1}^N b_{i,\ell} (\mathbf{e}^T \mathbf{g}_i) \mathbf{u}_{i,\ell} \right) \right] \\ &\quad + \frac{1}{\alpha} \sum_{\ell=1}^N (\nabla_{\mathbf{u}} \mathbf{J} \mathbf{u}_{\ell}) \mathbf{\Gamma}^{-1} (\mathbf{z}_{\ell} - \bar{\mathbf{z}}) \\ &\quad - \frac{1}{\alpha} \sum_{\ell=1}^N \sum_{i=1}^N b_{i,\ell} (\nabla_{\mathbf{u}} \mathbf{J} \mathbf{u}_{i,\ell}) \mathbf{\Gamma}^{-1} \mathbf{w}_i \end{aligned}$$

$$(3.20) \quad \mathbf{B}\hat{\boldsymbol{\theta}} = \sqrt{\alpha} \tilde{\mathbf{S}}_z^T \nabla_{\mathbf{u}, \mathbf{u}} \mathbf{J} \left(\sum_{i=1}^N \frac{\mathbf{e}^T \mathbf{g}_i}{\sqrt{\lambda_i}} \hat{\mathbf{u}}_i \right) + \sqrt{\alpha} \sum_{i=1}^N \frac{\nabla_{\mathbf{u}} \mathbf{J} \hat{\mathbf{u}}_i}{\sqrt{\lambda_i}} \mathbf{\Gamma}^{-1} \mathbf{w}_i$$

and

$$(3.21) \quad \mathbf{B}\tilde{\boldsymbol{\theta}} = \sum_{k=1}^{n-N+1} (\nabla_{\mathbf{u}} \mathbf{J} \tilde{\mathbf{u}}_k) \mathbf{\Gamma}^{-\frac{1}{2}} \tilde{\mathbf{z}}_k.$$

Hence, we may compute samples of the optimal solution as $\bar{\mathbf{z}} - \mathbf{H}^{-1} \mathbf{B}(\bar{\boldsymbol{\theta}} + \hat{\boldsymbol{\theta}} + \tilde{\boldsymbol{\theta}})$ without requiring computation in \mathbb{R}^p . Observe how (3.19)-(3.21) provides a systematic combination of high-fidelity data defining \mathbf{u}_{ℓ} and $\mathbf{u}_{i,\ell}$, the low-fidelity model in $\tilde{\mathbf{S}}_z^T$, prior information via \mathbf{L} and $\mathbf{\Gamma}$ (which appear in several terms in the expressions), and the optimization objective in $\nabla_{\mathbf{u}} \mathbf{J}$ and $\nabla_{\mathbf{u}, \mathbf{u}} \mathbf{J}$.

4. Algorithmic overview and computational cost analysis. This section presents an algorithmic overview to detail how quantities derived in the previous section may be computed efficiently, and the total cost to compute them. We organize into subsections which detail the computation of samples from the prior discrepancy, the posterior discrepancy, and the posterior optimal solution. In each subsection we provide a pseudo-code to summarize the algorithm and computational cost by counting the total number of linear system solves (in \mathbb{R}^m or \mathbb{R}^n). Since the number of high-fidelity forward solves N is small we consider computation in \mathbb{R}^N to be negligible.

4.1. Prior discrepancy samples. Using the factorization $\mathbf{M}_{\boldsymbol{\theta}}^{-1} = \mathbf{C}^{-T} \mathbf{C}^{-1}$, we derive an algorithm to draw prior samples of the model discrepancy. In particular, a prior sample of $\boldsymbol{\theta}$ is given by $\mathbf{C}^{-T} \boldsymbol{\omega}_p$, where $\boldsymbol{\omega}_p \sim \mathcal{N}(\mathbf{0}, \mathbf{I}_p)$. Evaluating the model discrepancy at such samples yields

$$\delta(\mathbf{z}, \mathbf{C}^{-T} \boldsymbol{\omega}_p) = \mathbf{L}^{-\frac{1}{2}} \boldsymbol{\omega}_0 + \mathbf{L}^{-\frac{1}{2}} \mathbf{\Omega} \mathbf{\Gamma}^{-\frac{1}{2}} (\mathbf{z} - \bar{\mathbf{z}})$$

where $\boldsymbol{\omega}_0 \in \mathbb{R}^m$ and $\mathbf{\Omega} \in \mathbb{R}^{m \times n}$ have entries which are independent identically distributed (i.i.d) samples from a standard normal distribution. To avoid sampling and forming the dense matrix $\mathbf{\Omega} \in \mathbb{R}^{m \times n}$, we evaluate $\delta(\mathbf{z}, \mathbf{C}^{-T} \boldsymbol{\omega})$ at particular \mathbf{z} 's sampled as $\mathbf{z} \sim \mathcal{N}(\bar{\mathbf{z}}, \mathbf{\Gamma})$. Such samples take the form $\mathbf{z} = \bar{\mathbf{z}} + \mathbf{\Gamma}^{\frac{1}{2}} \boldsymbol{\omega}_n$, where $\boldsymbol{\omega}_n \sim \mathcal{N}(\mathbf{0}, \mathbf{I}_n)$, and hence a prior discrepancy sample evaluated at \mathbf{z} takes the form

$$\delta(\bar{\mathbf{z}} + \mathbf{\Gamma}^{\frac{1}{2}} \boldsymbol{\omega}_n, \mathbf{C}^{-T} \boldsymbol{\omega}_p) = \mathbf{L}^{-\frac{1}{2}} (\boldsymbol{\omega}_0 + \mathbf{\Omega} \boldsymbol{\omega}_n).$$

Given a fixed ω_n , we sample discrepancies as $\delta(\bar{z} + \Gamma^{\frac{1}{2}}\omega_n, \mathbf{C}^{-T}\omega_p) = \mathbf{L}^{-\frac{1}{2}}\omega_m$, where $\omega_m \sim \mathcal{N}(\mathbf{0}, (1 + \omega_n^T \omega_n) \mathbf{I}_m)$ follows from taking sums and linear transformations of Gaussian random vectors. Thus, to compute S samples of \mathbf{z} and $\delta(\mathbf{z}, \boldsymbol{\theta})$ we apply $\mathbf{L}^{-\frac{1}{2}}$ and $\Gamma^{\frac{1}{2}}$ to S standard normal random vectors in \mathbb{R}^m and \mathbb{R}^n , respectively, and scale the resulting images of $\mathbf{L}^{-\frac{1}{2}}$. This is summarized in Algorithm 4.1.

Algorithm 4.1 Compute samples of the prior \mathbf{z} and discrepancy $\delta(\mathbf{z}, \boldsymbol{\theta})$.

```

1: Input: Number of desired samples  $S$ 
2: for  $s = 1, 2, \dots, S$  do
3:   Sample  $\omega_m \in \mathbb{R}^m$  and  $\omega_n \in \mathbb{R}^n$  with i.i.d. standard normal entries
4:   Compute:  $\mathbf{z}_s^{\text{prior}} = \bar{z} + \Gamma^{\frac{1}{2}}\omega_n \in \mathbb{R}^n$ 
5:    $\delta_s^{\text{prior}}(\mathbf{z}_s^{\text{prior}}) = \sqrt{1 + \omega_n^T \omega_n} \mathbf{L}^{-\frac{1}{2}}\omega_m$ 
6: end for
7:
8: Number of linear solves:  $\Gamma^{\frac{1}{2}}$   $\mathbf{L}^{-\frac{1}{2}}$ 
9:  $S$   $S$ 

```

4.2. Posterior discrepancy samples. To generate posterior samples, we compute $\Gamma^{-1}\mathbf{z}_\ell$, $\mathbf{L}^{-1}\mathbf{y}_\ell$, and $(\alpha\mathbf{L} + \lambda_i\mathbf{I})^{-1}\mathbf{L}^{-1}\mathbf{y}_\ell$, $\ell = 1, 2, \dots, N$, $i = 1, 2, \dots, N$, as a preprocessing step and store the resulting vectors. As with the prior, we simplify our analysis by evaluating at a specific inputs, namely the input data $\{\mathbf{z}_\ell\}_{\ell=1}^N$. Recalling the decomposition (3.16) into $\bar{\delta}$, $\hat{\delta}$, and $\tilde{\delta}$, and the observation that $\tilde{\delta}(\mathbf{z}_\ell) = 0$, we ignore the computation of $\tilde{\delta}$. Realizations of $\tilde{\delta}$ at other inputs will be the scaled versions of the prior discrepancy.

We compute $\bar{\delta}(\mathbf{z}_\ell)$ in closed form using precomputed data. Computing a sample of $\hat{\delta}(\mathbf{z}_\ell)$ requires N linear solves to apply $(\alpha\mathbf{L} + \lambda_i\mathbf{I})^{-\frac{1}{2}}$, $i = 1, 2, \dots, N$, to random vectors. This is summarized in Algorithm 4.2.

Algorithm 4.2 Compute posterior discrepancy samples.

```

1: Input: Number of desired samples  $S$ 
2: for  $\ell = 1, 2, \dots, N$  do
3:   Compute:  $\Gamma^{-1}\mathbf{z}_\ell$ 
4:    $\mathbf{L}^{-1}\mathbf{y}_\ell$ 
5:   for  $i = 1, 2, \dots, N$  do
6:     Compute  $(\alpha\mathbf{L} + \lambda_i\mathbf{I})^{-1}\mathbf{L}^{-1}\mathbf{y}_\ell$ 
7:   end for
8: end for
9: Evaluate  $\bar{\delta}(\mathbf{z}_\ell)$ ,  $\ell = 1, 2, \dots, N$ , using (3.17)
10: for  $s = 1, 2, \dots, S$  do
11:   for  $i = 1, 2, \dots, N$  do
12:     Sample  $\omega_m \in \mathbb{R}^m$  with i.i.d. standard normal entries
13:     Compute  $(\alpha\mathbf{L} + \lambda_i\mathbf{I})^{-\frac{1}{2}}\omega_m$ 
14:   end for
15:   Evaluate the  $s^{\text{th}}$  sample of  $\hat{\delta}(\mathbf{z}_\ell)$ ,  $\ell = 1, 2, \dots, N$ , using (3.18)
16: end for
17:
18: Number of linear solves:  $\Gamma^{-1}$   $\mathbf{L}^{-1}$   $(\alpha\mathbf{L} + \lambda_i\mathbf{I})^{-1}$   $(\alpha\mathbf{L} + \lambda_i\mathbf{I})^{-\frac{1}{2}}$ 
19:  $N$   $N$   $N^2$   $NS$ 

```

Note that the posterior discrepancy samples reveal the effect of α on our analysis. If the user computes S posterior samples and observes that they interpolate the data with little uncertainty then α may be increased to put less weight on the misfit. If the samples appear more like the prior samples than the data the user may decrease α to put more weight on the misfit. To generate S samples for a new α will require recomputing N^2 solves with $(\alpha\mathbf{L} + \lambda_i\mathbf{I})^{-1}$ and NS solves with $(\alpha\mathbf{L} + \lambda_i\mathbf{I})^{-\frac{1}{2}}$.

4.3. Posterior optimal solution samples. Given the computation of posterior discrepancy samples, this subsection details their propagation through $\mathbf{F}'_{\theta}(\mathbf{0})$ to get optimal solution posterior samples. The proposed approach begins with propagating posterior samples through \mathbf{B} and then applying $-\mathbf{H}^{-1}$ to the resulting vectors in \mathbb{R}^n . We use the decomposition $\bar{\theta} + \hat{\theta} + \tilde{\theta}$ of the samples, and demonstrate how to efficiently apply \mathbf{B} to each term.

Recalling the form of $\mathbf{B}\bar{\theta} \in \mathbb{R}^n$ in (3.19), observe that it may be computed using existing data which was precomputed in the posterior discrepancy sampling, along with matrix-vector products with $\nabla_{\mathbf{u},\mathbf{u}}\mathbf{J}$ and $\tilde{\mathbf{S}}_z^T$. This cost is dominated by the matrix-vector product with $\tilde{\mathbf{S}}_z^T$ which involves a linear system solve in \mathbb{R}^m .

To compute $\mathbf{B}\hat{\theta}$ as in (3.20), we leverage the data from computing posterior discrepancy samples and observe that the additional cost to compute $\mathbf{B}\hat{\theta}$ are matrix-vector products with $\nabla_{\mathbf{u},\mathbf{u}}\mathbf{J}$ and $\tilde{\mathbf{S}}_z^T$ per sample.

Lastly, computing $\mathbf{B}\tilde{\theta}$ using (3.21) involves linear combinations of the vectors $\Gamma^{-\frac{1}{2}}\tilde{\mathbf{z}}_k$ with coefficients

$$\nabla_{\mathbf{u}}\mathbf{J}\tilde{\mathbf{u}}_k = \nabla_{\mathbf{u}}\mathbf{J}\mathbf{L}^{-\frac{1}{2}}\nu_{N+k}.$$

With a naive implementation, this may be computationally intensive. However, the coefficients are normally distributed (scalar) random variables with mean 0 and variance $\nabla_{\mathbf{u}}\mathbf{J}\mathbf{L}^{-1}\nabla_{\mathbf{u}}\mathbf{J}^T$. Hence we may consider the equivalent sample

$$\sqrt{\nabla_{\mathbf{u}}\mathbf{J}\mathbf{L}^{-1}\nabla_{\mathbf{u}}\mathbf{J}^T}\Gamma^{-\frac{1}{2}}\sum_{k=1}^{n-N+1}c_k\tilde{\mathbf{z}}_k$$

where $c_k, k = 1, 2, \dots, n-N+1$, are i.i.d samples from a standard normal distribution. Recall that $\{\tilde{\mathbf{z}}_1, \tilde{\mathbf{z}}_2, \dots, \tilde{\mathbf{z}}_{n-N+1}\}$ is an orthonormal set of vectors which are orthogonal to $\mathcal{M} = \text{span}\{\Gamma^{-\frac{1}{2}}(\mathbf{z}_\ell - \bar{\mathbf{z}})\}_{\ell=2}^N$, and let $\{\tilde{\mathbf{z}}_1^{\mathcal{M}}, \tilde{\mathbf{z}}_2^{\mathcal{M}}, \dots, \tilde{\mathbf{z}}_{N-1}^{\mathcal{M}}\}$ be an orthonormal basis for \mathcal{M} . Letting $\mathbf{P}_{\mathcal{M}^\perp}$ be a projector onto \mathcal{M}^\perp , the orthogonal complement of \mathcal{M} , i.e. $\mathbf{P}_{\mathcal{M}^\perp}\tilde{\mathbf{z}}_k = \tilde{\mathbf{z}}_k$ and $\mathbf{P}_{\mathcal{M}^\perp}\tilde{\mathbf{z}}_k^{\mathcal{M}} = \mathbf{0}$, we may sample $\mathbf{B}\tilde{\theta}$ as

$$\sqrt{\nabla_{\mathbf{u}}\mathbf{J}\mathbf{L}^{-1}\nabla_{\mathbf{u}}\mathbf{J}^T}\Gamma^{-\frac{1}{2}}\mathbf{P}_{\mathcal{M}^\perp}\left(\sum_{k=1}^{n-N+1}c_k\tilde{\mathbf{z}}_k + \sum_{k=1}^{N-1}c_{n-N+1+k}\tilde{\mathbf{z}}_k^{\mathcal{M}}\right),$$

where $c_{n-N+1+k}$ are independent standard normal random variables. Since

$$\{\tilde{\mathbf{z}}_1, \tilde{\mathbf{z}}_2, \dots, \tilde{\mathbf{z}}_{n-N+1}\} \cup \{\tilde{\mathbf{z}}_1^{\mathcal{M}}, \tilde{\mathbf{z}}_2^{\mathcal{M}}, \dots, \tilde{\mathbf{z}}_{N-1}^{\mathcal{M}}\}$$

is an orthonormal basis for \mathbb{R}^n , the sum over an orthonormal basis with i.i.d standard normal coefficients corresponds to rotating a Gaussian, which does not change its distribution. Hence we may equivalently compute samples as

$$\sqrt{\nabla_{\mathbf{u}}\mathbf{J}\mathbf{L}^{-1}\nabla_{\mathbf{u}}\mathbf{J}^T}\Gamma^{-\frac{1}{2}}\mathbf{P}_{\mathcal{M}^\perp}\omega_n$$

where $\boldsymbol{\omega}_n \sim \mathcal{N}(\mathbf{0}, \mathbf{I}_n)$. This alleviates the need to compute $\{\tilde{\mathbf{z}}_1, \tilde{\mathbf{z}}_2, \dots, \tilde{\mathbf{z}}_{n-N+1}\}$ since $\mathbf{P}_{\mathcal{M}^\perp}$ can be written in terms of $\{\boldsymbol{\Gamma}^{-\frac{1}{2}}(\mathbf{z}_\ell - \bar{\mathbf{z}})\}_{\ell=2}^N$. Using properties of orthogonal projectors we arrive at the expression to sample $\mathbf{B}\boldsymbol{\theta}$ as

$$(4.1) \quad \sqrt{\nabla_{\mathbf{u}} \mathbf{J} \mathbf{L}^{-1} \nabla_{\mathbf{u}} \mathbf{J}^T} \left(\mathbf{I}_n - \boldsymbol{\Gamma}^{-1} \hat{\mathbf{Z}} \left(\hat{\mathbf{Z}}^T \boldsymbol{\Gamma}^{-1} \hat{\mathbf{Z}} \right)^{-1} \hat{\mathbf{Z}}^T \right) \boldsymbol{\Gamma}^{-\frac{1}{2}} \boldsymbol{\omega}_n$$

where

$$\hat{\mathbf{Z}} = \begin{pmatrix} (\mathbf{z}_2 - \bar{\mathbf{z}}) & (\mathbf{z}_3 - \bar{\mathbf{z}}) & \dots & (\mathbf{z}_N - \bar{\mathbf{z}}) \end{pmatrix} \in \mathbb{R}^{n \times (N-1)}.$$

Since $\boldsymbol{\Gamma}^{-1} \mathbf{z}_\ell$, $\ell = 1, 2, \dots, N$ has already been computed we may form $\boldsymbol{\Gamma}^{-1} \hat{\mathbf{Z}}$ with no additional solves, and the inversion of $\hat{\mathbf{Z}}^T \boldsymbol{\Gamma}^{-1} \hat{\mathbf{Z}}$ is done on a $N \times N$ matrix which we assume to have negligible cost. The only additional cost is computing $\boldsymbol{\Gamma}^{-\frac{1}{2}} \boldsymbol{\omega}_n$ for each sample. For problems where n is large and N is small, this provides a considerable computational savings relative to explicitly forming $\{\tilde{\mathbf{z}}_1, \tilde{\mathbf{z}}_2, \dots, \tilde{\mathbf{z}}_{n-N+1}\}$.

Sampling from the optimal solution posterior is summarized in Algorithm 4.3. We emphasize the reduced cost thanks to the wealth of precomputed data from the prior and posterior discrepancy sampling.

Algorithm 4.3 Compute optimal solution posterior samples.

- 1: Input: Number of desired samples S
 - 2: Compute: $\mathbf{L}^{-1} \nabla_{\mathbf{u}} \mathbf{J}^T$
 - 3: $\mathbf{B}\bar{\boldsymbol{\theta}}$ using (3.19) by applying $\tilde{\mathbf{S}}_z^T \nabla_{\mathbf{u}, \mathbf{u}} \mathbf{J}$ to precomputed data
 - 4: $-\mathbf{H}^{-1} \mathbf{B}\bar{\boldsymbol{\theta}}$
 - 5: **for** $s = 1, 2, \dots, S$ **do**
 - 6: Compute: $\mathbf{B}\boldsymbol{\theta}$ using (3.20) by applying $\tilde{\mathbf{S}}_z^T \nabla_{\mathbf{u}, \mathbf{u}} \mathbf{J}$ to precomputed data
 - 7: $\boldsymbol{\Gamma}^{-\frac{1}{2}} \boldsymbol{\omega}_n$ for a sample $\boldsymbol{\Omega}_n \sim \mathcal{N}(\mathbf{0}, \mathbf{I}_n)$
 - 8: $\mathbf{B}\tilde{\boldsymbol{\theta}}$ using (4.1) with precomputed data
 - 9: $-\mathbf{H}^{-1}(\mathbf{B}\boldsymbol{\theta} + \mathbf{B}\tilde{\boldsymbol{\theta}})$
 - 10: **end for**
 - 11:

 - 12: Number of linear solves: \mathbf{L}^{-1} $\boldsymbol{\Gamma}^{-\frac{1}{2}}$ $\tilde{\mathbf{S}}_z^T$ \mathbf{H}^{-1}
 - 13: 1 S $S + 1$ $S + 1$
-

5. Numerical results. We present two examples to demonstrate our proposed method. The first, an illustrative 1D control example, where model discrepancy arises from a failure to include advection, and second, an application to fluid flow in 2D where a Stokes model is used as the low-fidelity approximation of a Navier-Stokes model.

5.1. Illustrative example. Consider a 1D steady state control problem. It corresponds to determining the optimal source to achieve a target state profile. Specially, the optimization problem

$$\min_z \frac{1}{2} \int_0^1 (\tilde{S}(z) - T(x))^2 dx + \frac{\beta_1}{2} \int_0^1 z(x)^2 dx + \frac{\beta_2}{2} \int_0^1 z'(x)^2 dx$$

where $T(x) = 50 - 30(x - 0.5)^2$ is the target, $z : [0, 1] \rightarrow \mathbb{R}$ is a source controller, $\beta_1 = 10$ and $\beta_2 = 10^{-2}$ are regularization coefficients, and $\tilde{S}(z)$ is the solution operator

for the diffusion equation

$$\begin{aligned} -\kappa u'' &= z && \text{on } (0, 1) \\ \kappa u' &= hu && \text{on } \{0, 1\} \end{aligned}$$

with Robin boundary condition. Assume that the diffusion model is erroneous in that it lacks advection. We consider the high-fidelity model to be

$$\begin{aligned} -\kappa u'' + vu' &= z && \text{on } (0, 1) \\ \kappa u' &= hu && \text{on } \{0, 1\} \end{aligned}$$

whose solution operator is $S(z)$. We take parameter values $\kappa = 1$, $v = 0.5$, and $h = 2$.

Optimization. After discretizing with linear finite elements on a uniform mesh of 200 nodes, i.e. $m = n = 200$, we solve both high and low-fidelity optimization problems to illustrate the effect of model error, i.e. missing the advection term. We observe a considerable difference in the optimal sources, shown in Figure 3. Since advection moves the state from left to right, including advection in the model resulted in a source skewed to the left.

Prior model discrepancy. To define the discrepancy prior, the \mathbf{z} covariance matrix is taken as $\mathbf{\Gamma} = (\mathbf{D}_z \mathbf{M}^{-1} \mathbf{D}_z)^{-1}$, where \mathbf{D}_z is the discretization of the elliptic operator $s_z(-\epsilon_z \Delta + \mathcal{I})$, $s_z = 1$ and $\epsilon_z = 10^{-5}$, equipped with zero Neumann boundary conditions, and \mathbf{M} is the mass matrix arising from the finite element discretization. In a similar fashion, the prior state discrepancy is taken as a zero mean Gaussian with covariance $\mathbf{L}^{-1} = (\mathbf{D}_u \mathbf{M}^{-1} \mathbf{D}_u)^{-1}$, where \mathbf{D}_u is the discretization of the elliptic operator $s_u(-\epsilon_u \Delta + \mathcal{I})$, $s_u = 15$ and $\epsilon_u = 5 \times 10^{-3}$, equipped with zero Neumann boundary conditions. Our choice of prior covariances are common in PDE-constrained Bayesian inverse problems because of the interpretability of their parameters, theoretical properties of the prior samples, and computational convenience of efficient linear solves and matrix factorizations for sampling. Executing Algorithm 4.1, we generate prior samples which are displayed in the left and center panels of Figure 2. These samples provide a visual interpretation of the prior to assist in choosing s_z , ϵ_z , s_u , and ϵ_u , which play an important role defining length scales in the analysis.

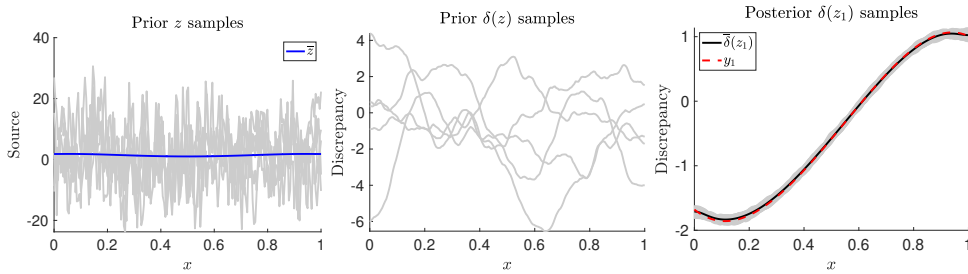


FIG. 2. Five samples from the prior source (left panel) and prior model discrepancy (center panel). The right panel shows the posterior distribution of δ evaluated at $\mathbf{z} = \mathbf{z}_1$. Its mean is given by the black line, samples are denoted using grey lines, and the discrepancy data \mathbf{y}_1 is shown by the broken red lines.

Posterior model discrepancy. We evaluate the high-fidelity model twice to generate $N = 2$ data points $\{\mathbf{z}_\ell, \mathbf{y}_\ell\}_{\ell=1}^2$. Algorithm 4.2 is executed, with the noise covariance $\alpha = 0.01$, to fit the model discrepancy. The right panel of Figure 2 displays

posterior samples of δ evaluated at \mathbf{z}_1 . We observe that the means match the data well and the posterior samples are concentrated around the mean. This is unsurprising given that $\mathbf{S}(\mathbf{z}) - \tilde{\mathbf{S}}(\mathbf{z})$ is a linear function of \mathbf{z} and α was taken small enough to encourage trust in the data. As with the prior, plotting the posterior discrepancy enables visual analysis of the user specified noise covariance α . If α is taken too small we would see negligible uncertainty in the posterior, whereas if α is taken too large we would see the posterior discrepancy mean being close to zero as the inversion puts more weight on the prior than the data. Visualizing the posterior discrepancy provides an efficient way to tune α before the more computationally intensive generation of optimal solution posterior samples.

Posterior optimal solution. Executing Algorithm 4.3 to propagate the posterior model discrepancy through the post-optimality sensitivity operator, we arrive at a posterior distribution for the optimal source which is shown in Figure 3. We observe that the posterior mean for the optimal solution is much closer to the high-fidelity solution \mathbf{z}^* than our nominal low-fidelity solution $\bar{\mathbf{z}}$. Hence using the low-fidelity optimization problem along with two high-fidelity forward solves, we are able to find a good approximation of the high-fidelity optimal solution. Further, the greatest errors (difference in the posterior mean and high-fidelity solution) occur near the boundaries and this error is captured by the wider range of posterior uncertainty in those regions.

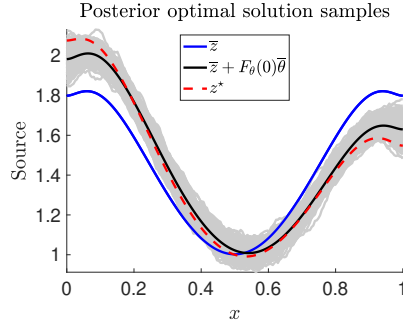


FIG. 3. Posterior distribution of the optimal source \mathbf{z} . The mean is given by the black line and samples are denoted using grey lines. The low and high-fidelity solutions $\bar{\mathbf{z}}$ and \mathbf{z}^* are shown by the blue and broken red lines, respectively.

5.2. Control of viscous fluid flow. In this subsection the proposed approach is demonstrated to control viscous fluid flow. In particular, we consider the high-fidelity model to be governed by the Navier-Stokes equation, but because of the high viscosity of the fluid, the Stokes equation is used as a low-fidelity model to simplify the computation. In particular, we seek a distributed controller $\mathbf{z} = (z_x, z_y)$ to minimize the vertical fluid flow. The low-fidelity optimization problem is

$$\min_{\mathbf{z}} \frac{1}{2} \int_{\mathcal{X}} \tilde{\mathbf{v}}_y(z)^2 + \frac{\beta_1}{2} \int_{\Omega} (z_x^2 + z_y^2) + \frac{\beta_2}{2} \int_{\Omega} (\|\nabla z_x\|^2 + \|\nabla z_y\|^2)$$

where $\tilde{\mathbf{v}}(z) = (\tilde{v}_x(z), \tilde{v}_y(z))$ is the velocity solution operator for the Stokes equation

$$\begin{aligned} -\mu \nabla \mathbf{v} + \nabla p &= \mathbf{g} + \mathbf{z} && \text{on } \Omega \\ \nabla \cdot \mathbf{v} &= 0 && \text{on } \Omega \end{aligned}$$

where $\Omega = (0, 1)^2$ and $\chi = (0, 1) \times (0, 0.5)$. The flow is driven by the effect of gravity $\mathbf{g} = (0, 9.81)$ and the inflow boundary conditions

$$v_x(0, y) = 6y(1 - y) \quad \text{and} \quad v_y(x, 1) = -2 \sin(2\pi x)^2,$$

and has viscosity $\mu = 0.5$. We solve the optimization problem with regularization coefficients $\beta_1 = \beta_2 = 10^{-5}$. The high-fidelity Navier-Stokes model

$$\begin{aligned} -\mu \nabla \mathbf{v} + (\mathbf{v} \cdot \nabla) \mathbf{v} + \nabla p &= \mathbf{g} + \mathbf{z} && \text{on } \Omega \\ \nabla \cdot \mathbf{v} &= 0 && \text{on } \Omega \end{aligned}$$

includes the nonlinear convective term omitted from the Stokes equation.

Optimization. The PDE is discretized with Taylor-Hood elements with $m = 23,003$ degrees of freedom to discretize the three state variables v_x , v_y , and p . Figure 4 displays the uncontrolled and optimality controlled solutions of the Stokes equation. The inflow from the left and above, combined with the force of gravity, produce a flow field with high downward velocity in the lower region of the domain. The objective is minimizing the speed of this flow and the efficacy of the controller is apparent from the center column of Figure 4. However, the Navier-Stokes solution evaluated at the optimal controller exhibits faster flows as shown in the left panel of Figure 7.

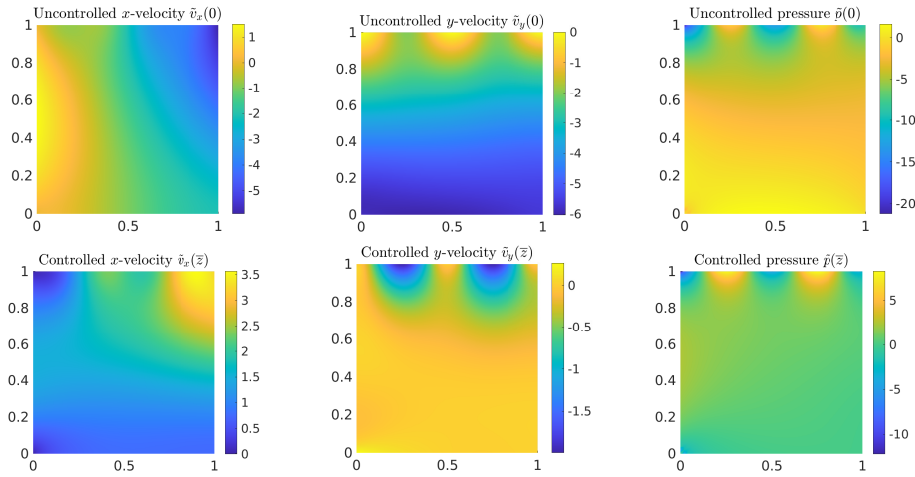


FIG. 4. Uncontrolled (top) and controlled (bottom) state solution for the Stokes equation. The x -velocity v_x , y -velocity v_y , and pressure p are plotted from left to right.

Prior model discrepancy. Similar to the previous example, we define the prior covariances $\mathbf{\Gamma}$ and \mathbf{L}^{-1} as the square of the inverse of elliptic differential operators. However, to mitigate the effect of high boundary variance in the prior we follow [14] by imposing a Robin boundary condition which is optimized to reduce the boundary effect. This condition is not sufficient to completely eliminate the inflated variance near the boundary, so we complement it with a rescaling of the covariance based on a point-wise variance estimate using 100 samples. The prior controller covariance is $\mathbf{\Gamma} = \mathbf{s}_z^2 (\mathbf{E}_z^{-\frac{1}{2}} \mathbf{D}_z \mathbf{M}_z^{-1} \mathbf{D}_z \mathbf{E}_z^{-\frac{1}{2}})^{-1}$, where \mathbf{D}_z is the discretization of the elliptic operator $(-\epsilon_z \Delta + \mathcal{I})$, $s_z = 13$ and $\epsilon_z = 10^{-4}$, and \mathbf{E}_z is a diagonal matrix which

approximates the point-wise variance of $(\mathbf{D}_z \mathbf{M}_z^{-1} \mathbf{D}_z)^{-1}$, and \mathbf{M}_z is the mass matrix for the controller discretization. Similarly, $\mathbf{L}^{-1} = \mathbf{s}_u^2 (\mathbf{E}_u^{-\frac{1}{2}} \mathbf{D}_u \mathbf{M}_u^{-1} \mathbf{D}_u \mathbf{E}_u^{-\frac{1}{2}})^{-1}$, where \mathbf{D}_u is the discretization of the elliptic operator $(-\epsilon_u \Delta + \mathcal{I})$, $s_u = 1$ and $\epsilon_u = 0.2$, and \mathbf{E}_u is a diagonal matrix which approximates the point-wise variance of $(\mathbf{D}_u \mathbf{M}_u^{-1} \mathbf{D}_u)^{-1}$, and \mathbf{M}_u is the mass matrix for the state discretization. We omit showing prior samples for conciseness, but emphasize that the interpretability of the elliptic operator allowed for easy specification of the variance and correlation lengths to ensure that the prior is reflective of the physical characteristics of \mathbf{z} and δ .

To facilitate efficient computation, especially inversion of the shifted linear systems $\alpha \mathbf{L} + \lambda_i \mathbf{I}$ and its square root, we compute the generalized singular value decomposition of \mathbf{D}_u^{-1} in the \mathbf{M}_u and \mathbf{E}_u^{-1} inner product, which after algebraic manipulations gives the eigenvalue decomposition of \mathbf{L}^{-1} . The subsequent linear solves involving \mathbf{L} may be efficiently approximated using the truncated eigenvalue decomposition and the error in the approximation is controlled by the rank, which we take to be 1000, ensuring a relative truncation error of $\mathcal{O}(10^{-3})$.

Posterior model discrepancy. We evaluate the Navier-Stokes equation at the optimal Stokes controller to generate the data point $(\mathbf{z}_1, \mathbf{y}_1)$ to fit the model discrepancy, i.e. $N = 1$. Taking $\alpha = 1.0$, we solve the Bayesian inverse problem to calibrate $\delta(\mathbf{z})$. Figure 5 displays the posterior mean of δ evaluated at the controller \mathbf{z}_1 . We observe that it matches the data well, as we expect. Posterior samples to characterize uncertainty were also generated, but are omitted from the article for conciseness.

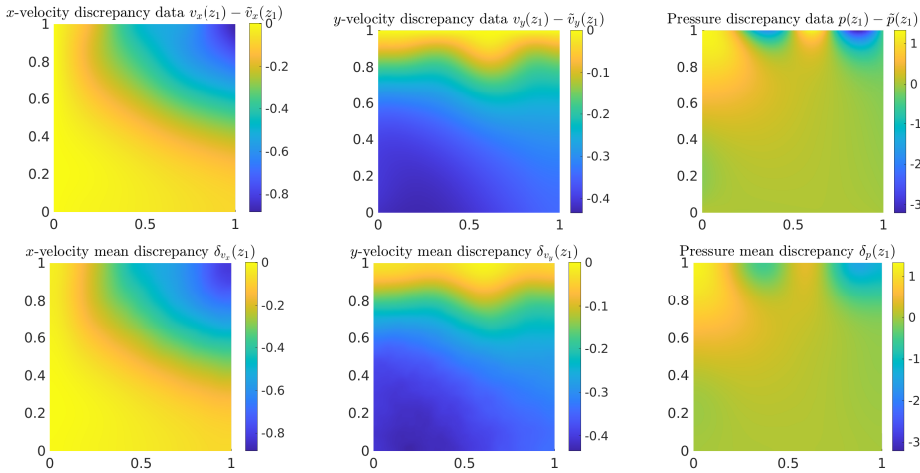


FIG. 5. Observed data (top) and mean fit (bottom) for the state discrepancy. The x -velocity v_x , y -velocity v_y , and pressure p are plotted from left to right.

Posterior optimal solution. Lastly, the mean and 100 samples from the posterior discrepancy are propagated through the post-optimality sensitivity operator to produce the posterior optimal solution. To illustrate the benefit of the controller update, Figure 6 displays the optimal controller generated by solving the Stokes problem, the mean of the optimal solution posterior, and the optimal controller generated by solving the control problem constrained by the Navier-Stokes equation. The latter controller is generally not available in practice, but we compute and display it here for validation. By comparing across the rows of Figure 6, we see that calibrating

the discrepancy with $N = 1$ high-fidelity forward solves significantly improves the controller, particularly the y -velocity controller in the left region of the domain.

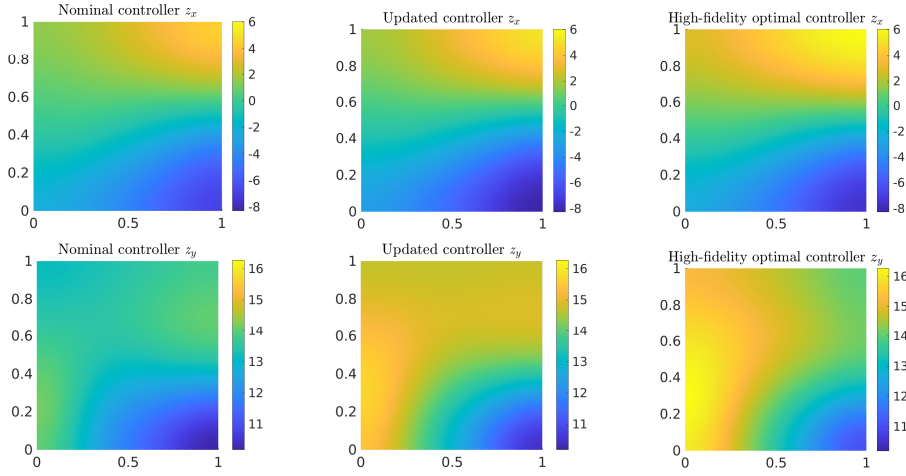


FIG. 6. Controllers acting on the x -velocity component (top) and the y -velocity component (bottom). The left column is the nominal control solution, the center column is the mean of the posterior optimal solution, and the right column is the optimal solution computed by solving the control problem constrained by the Navier-Stokes model.

To further quantify the benefit of the controller update, Figure 7 displays the vertical velocity v_y of the Navier-Stokes solution when evaluated at the Stokes optimal controller (left), the updated optimal controller (center), and the Navier-Stokes optimal controller (right). The performance improvement is significant given that it was achieved using only $N = 1$ Navier-Stokes solve to update the Stokes solution. The comparison is further quantified in Table 1 which displays the value of the objective function, evaluated using the Navier-Stokes model, for each of the controllers. The controller updated decreased the value of the objective by two order of magnitude relative to the nominal Stokes control solution, while falling one order of magnitude short of the best possible value, the Navier-Stokes optimal control solution.

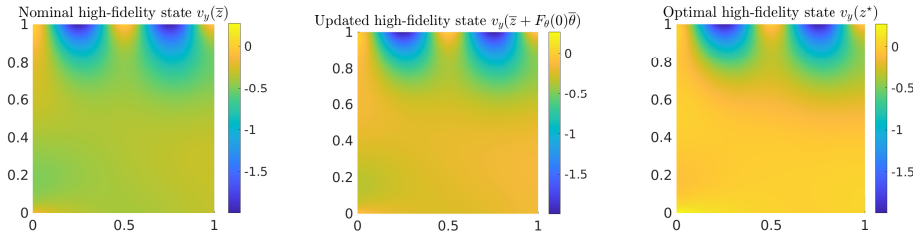


FIG. 7. Vertical velocity state solutions corresponding to: Navier-Stokes solve with nominal control (left), Navier-Stokes solve with updated control (center), and Navier-Stokes with optimal control (right).

Lastly, with a recognition that computing the optimal controller update is underdetermined using only one high-fidelity solve, Figure 8 displays the posterior covariance of the optimal controller. Due to its high-dimensionality, we visualize the uncertainty by performing principle component analysis (PCA) on the 100 posterior

Controller	Objective Function Value
\bar{z}	3.13×10^0
$\bar{z} + \mathbf{F}'_{\theta}(\mathbf{0})\bar{\theta}$	1.39×10^{-2}
z^*	2.24×10^{-3}

TABLE 1

Value of the objective function $J(S(z), z)$, where $S(z)$ is the Navier-Stokes solution operator.

samples and plot the leading four principle components (or modes). Each row in Figure 8 corresponds to a principle component, with the left column showing a histogram of the coefficient corresponding to the given mode, and the center (z_x) and right (z_y) columns showing the modes. The black vertical line indicates the mean of the optimal solution posterior, which is always zero since the distribution is centered. The blue and red vertical lines indicate the coefficients of the nominal Stokes optimal controller and the Naiver-Stokes optimal controller, respectively, when they are centered and projected onto the PCA mode. Ideally, the Naiver-Stokes optimal controller (the red line) should be in a high probability region. This is true in the leading four modes shown in Figure 8, but is not true for all of the modes. Having the Naiver-Stokes solution lie outside the high probably region for some modes is unsurprising given that the distribution was calibrated using only $N = 1$ high-fidelity forward solve.

6. Conclusion. It is common that high-fidelity models are too computationally intensive and/or their implementation does not allow efficient optimization, for instance, it may be difficult to implement adjoints to enable efficient derivative computations. In such cases, current practice is to construct low(er)-fidelity models through either simplifications of the equations from physics assumptions, or reduced order modeling techniques to approximate the high-fidelity model at a lower computational cost. The lower-fidelity model is used to constrain an optimization problem and its solution is assessed by evaluating the high-fidelity model a small number of times. However, these high-fidelity solves may be used for more than assessing the quality of the optimal solution. This article provides a framework which systematically uses the high-fidelity data to improve the optimal solution, without requiring any additional access to the high-fidelity solver. We have demonstrated how the optimal solution can be improved and uncertainty in it can be estimated by coupling a Bayesian approach to model discrepancy estimation with post-optimality sensitivity analysis.

Our proposed approach is computationally scalable thanks to judicious manipulations of linear algebra to enable closed form expressions for posterior samples. These efficiencies were discovered by taking a wholistic perspective which considered every aspect of the problem formulation (discrepancy representation, Gaussian prior and likelihood, post-optimality sensitivity operator, and the resulting matrix factorizations) to develop a mathematically rigorous and computationally advantageous approach. The fundamental assumption is a linear approximation of the model discrepancy to optimal solution mapping. However, as we demonstrated, this can provide considerable improvements for nonlinear PDE-constrained optimization problems with high-dimensional optimization variables.

Since we consider a Bayesian inverse problem to characterize the model discrepancy in a limited data setting, the prior distribution plays an important role in our analysis. By leveraging developments in the infinite dimensional Bayesian inverse problems literature, we have proposed a prior on the discrepancy which is interpretable and computationally efficient. The algorithm requires some user specified

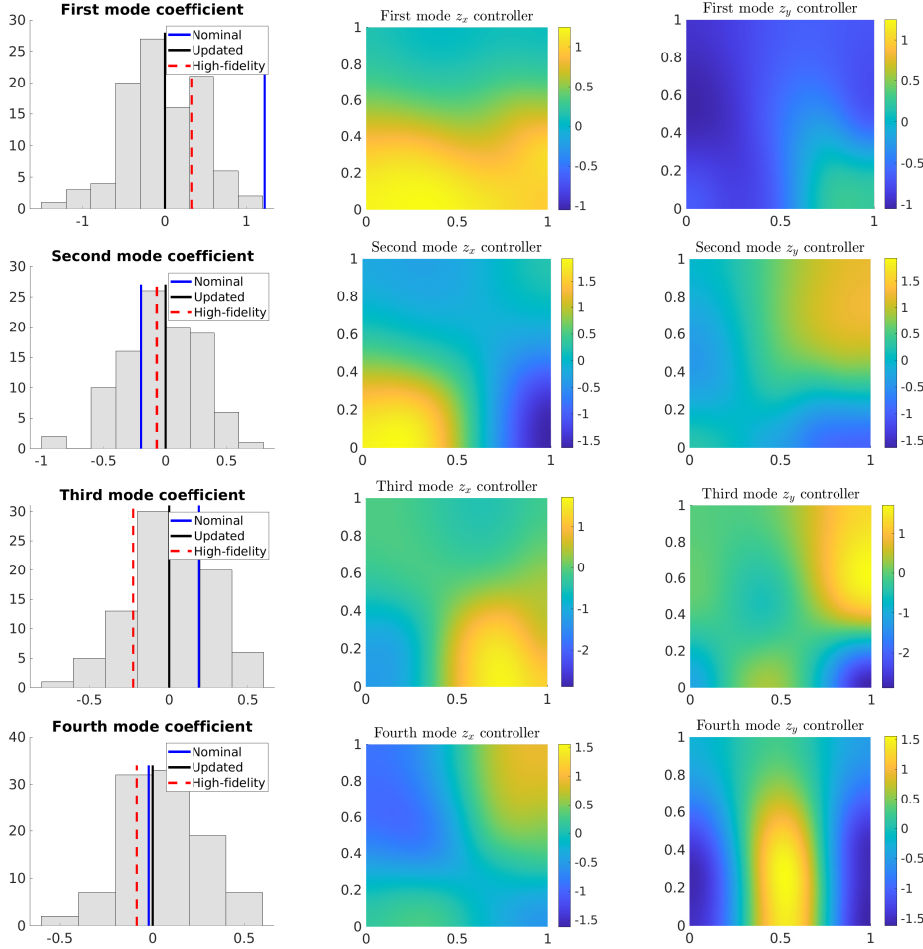


FIG. 8. Representation of uncertainty in the optimal solution posterior. Principal component analysis was performed on 100 posterior optimal solution samples. The four leading principal components (or modes) are shown in the rows. The first four modes capture approximately 84% of the posterior variance. The left column is a histogram showing the magnitude of the projection of the samples (minus the posterior mean) onto the mode. The projection of the nominal, updated, and high-fidelity controllers (minus the posterior mean) are indicated by the vertical lines. The projection of the updated controller equals zero for all modes because the data was centered around it.

parameters related to length scales, smoothness, and approximation errors; however, the analysis provides clear interpretations for how these choices influence the resulting posterior distribution.

There are many potential applications of our analysis including, but not limited too, (1) using models in three spatial dimensions to improve optimal solutions computed using models in two spatial dimensions, (2) using multi-scale models to improve solutions computed using homogenized models, (3) using coupled systems to improve optimal solutions computed using only a subset of the system, and (4) using high-fidelity data from controlled experiments in place of a high-fidelity model to improve design or control strategies. Other mathematical questions regarding how and when to query the high-fidelity model also remain and are the topic of ongoing research.

Acknowledgements. This paper describes objective technical results and analysis. Any subjective views or opinions that might be expressed in the paper do not necessarily represent the views of the U.S. Department of Energy or the United States Government. Sandia National Laboratories is a multimission laboratory managed and operated by National Technology and Engineering Solutions of Sandia LLC, a wholly owned subsidiary of Honeywell International, Inc., for the U.S. Department of Energy’s National Nuclear Security Administration under contract DE-NA-0003525. SAND2022-14144 O.

REFERENCES

- [1] N. ALEXANDROV, J. D. JR., R. LEWIS, AND V. TORCZON, *A trust-region framework for managing the use of approximation models in optimization*, Structural Optimization, 15 (1998), pp. 16–23.
- [2] H. ANTIL, D. P. KOURI, M. LACASSE, AND D. RIDZAL, eds., *Frontiers in PDE-Constrained Optimization*, Springer, 2018.
- [3] P. D. ARENDT, D. W. APLEY, AND W. CHEN, *Quantification of model uncertainty: Calibration, model discrepancy, and identifiability*, Journal of Mechanical Design, 134 (2012).
- [4] U. M. ASCHER AND E. HABER, *Grid refinement and scaling for distributed parameter estimation problems*, Inverse Problems, 17 (2001), pp. 571–590.
- [5] L. BIEGLER, G. BIROS, O. GHATTAS, M. HEINKENSCHLOSS, D. KEYES, B. MALLICK, Y. MARZOUK, L. TENORIO, B. VAN BLOEMEN WAANDERS, AND K. WILLCOX, eds., *Large-Scale Inverse Problems and Quantification of Uncertainty*, John Wiley and Sons, 2011.
- [6] L. T. BIEGLER, O. GHATTAS, M. HEINKENSCHLOSS, D. KEYES, AND B. VAN BLOEMEN WAANDERS, eds., *Real-Time PDE-Constrained Optimization*, vol. 3, SIAM Computational Science and Engineering, 2007.
- [7] G. BIROS AND O. GHATTAS, *Parallel Lagrange-Newton-Krylov-Schur methods for PDE-constrained optimization. Parts I-II*, SIAM J. Sci. Comput., 27 (2005), pp. 687–738.
- [8] J. F. BONNANS AND A. SHAPIRO, *Optimization problems with perturbations: A guided tour*, SIAM Review, 40 (1998), pp. 228–264.
- [9] A. BORZI, *High-order discretization and multigrid solution of elliptic nonlinear constrained optimal control problems*, J. Comp. Applied Math, 200 (2007), pp. 67–85.
- [10] K. BRANDES AND R. GRIESSE, *Quantitative stability analysis of optimal solutions in PDE-constrained optimization*, Journal of Computational and Applied Mathematics, 206 (2007), pp. 908–926.
- [11] J. BRYNJARSDÓTTIR AND A. O’HAGAN, *Learning about physical parameters: the importance of model discrepancy*, Inverse Problems, 30 (2014).
- [12] D. E. BRYSON AND M. P. RUMPFKEIL, *Multifidelity quasi-newton method for design optimization*, AIAA JOURNAL, 56 (2018).
- [13] T. BUI-THANH, O. GHATTAS, J. MARTIN, AND G. STADLER, *A computational framework for infinite-dimensional bayesian inverse problems. Part I: The linearized case, with applications to global seismic inversion*, SIAM Journal on Scientific Computing, 35 (2013), pp. A2494–A2523.
- [14] Y. DAON AND G. STADLER, *Mitigating the influence of the boundary on pde-based covariance operators*, Inverse Problems and Imaging, 12 (2018), pp. 1083–1102.
- [15] A. V. FIACCO AND A. GHAEMI, *Sensitivity analysis of a nonlinear structural design problem*, Computers and Operations Research, 9 (1982), pp. 29–55.
- [16] P. GARDNER, T. ROGERS, C. LORD, AND R. BARTHORPE, *Learning model discrepancy: A gaussian process and sampling-based approach*, Mechanical Systems and Signal Processing, 152 (2021).
- [17] A. A. GORODETSKY, G. GERACI, M. S. ELDERED, AND J. D. JAKEMAN, *A generalized approximate control variate framework for multifidelity uncertainty quantification*, Journal of Computational Physics, 408 (2020).
- [18] R. GRIESSE, *Parametric sensitivity analysis in optimal control of a reaction-diffusion system – part II: practical methods and examples*, Optimization Methods and Software, 19 (2004), pp. 217–242.
- [19] R. GRIESSE, *Parametric sensitivity analysis in optimal control of a reaction diffusion system. I. solution differentiability*, Numerical Functional Analysis and Optimization, 25 (2004), pp. 93–117.
- [20] E. HABER AND U. M. ASCHER, *Preconditioned all-at-once methods for large, sparse parameter*

- estimation problems*, Inverse Problems, 17 (2001), pp. 1847–1864.
- [21] J. HART AND B. VAN BLOEMEN WAANDERS, *Enabling hyper-differential sensitivity analysis for ill-posed inverse problems*, arXiv:2106.11813, (2021).
- [22] J. HART AND B. VAN BLOEMEN WAANDERS, *Hyper-differential sensitivity analysis with respect to model discrepancy: Mathematics and computation*, Preprint, (2022).
- [23] J. HART, B. VAN BLOEMEN WAANDERS, AND R. HERTZOG, *Hyper-differential sensitivity analysis of uncertain parameters in PDE-constrained optimization*, International Journal for Uncertainty Quantification, 10 (2020), pp. 225–248.
- [24] J. HART, B. VAN BLOEMEN WAANDERS, L. HOOD, AND J. PARISH, *Sensitivity driven experimental design to facilitate control of dynamical systems*, Submitted. arXiv: <https://arxiv.org/abs/2202.03312>, (2022).
- [25] S. B. HAZRA AND V. SCHULZ, *Simultaneous pseudo-timestepping for aerodynamic shape optimization problems with state constraints*, SIAM J. Sci. Comput., 28 (2006), pp. 1078–1099.
- [26] D. HIGDON, J. GATTIKER, B. WILLIAMS, AND M. RIGHTLEY, *Computer model calibration using high-dimensional output*, Journal of the American Statistical Association, 103 (2008), pp. 570–583.
- [27] M. HINTERMULLER AND L. N. VICENTE, *Space mapping for optimal control of partial differential equations*, SIAM J. Opt., 15 (2005), pp. 1002–1025.
- [28] M. HINZE, R. PINNAU, M. ULBRICH, AND S. ULBRICH, *Optimization with PDE Constraints*, Springer, 2009.
- [29] M. C. KENNEDY AND A. O’HAGAN, *Bayesian calibration of computer models*, Journal of the Royal Statistical Society, 63 (2001), pp. 425–464.
- [30] M. H. L. T. BIEGLER, O. GHATTAS AND B. VAN BLOEMEN WAANDERS, eds., *Large-Scale PDE-Constrained Optimization*, vol. 30, Springer-Verlag Lecture Notes in Computational Science and Engineering, 2003.
- [31] C. D. LAIRD, L. T. BIEGLER, B. VAN BLOEMEN WAANDERS, AND R. A. BARTLETT, *Time dependent contaminant source determination for municipal water networks using large scale optimization*, ASCE J. Water Res. Mgt. Plan., (2005), pp. 125–134.
- [32] Y. LING, J. MULLINS, AND S. MAHADEVAN, *Selection of model discrepancy priors in bayesian calibration*, Journal of Computational Physics, 276 (2014), pp. 665–680.
- [33] K. A. MAUPIN AND L. P. SWILER, *Model discrepancy calibration across experimental settings*, Reliability Engineering & System Safety, 200 (2020).
- [34] F. MENHORN, G. GERACI, D. T. SEIDL, M. S. ELDRRED, R. KING, H.-J. BUNGARTZ, AND Y. MARZOUK, *Higher moment multilevel estimators for optimization under uncertainty applied to wind plant design*, AIAA SciTech Forum, 2020.
- [35] L. W. NG AND K. E. WILLCOX, *Multifidelity approaches for optimization under uncertainty*, International Journal for Numerical Methods in Engineering, (2014).
- [36] J. OAKLEY AND A. O’HAGAN, *Bayesian inference for the uncertainty distribution of computer model outputs*, Biometrika, 89 (2002), pp. 769–784.
- [37] B. PEHERSTORFER, K. WILLCOX, AND M. GUNZBURGER, *Survey of multifidelity methods in uncertainty propagation, inference, and optimization*, SIAM Review, 60 (2018), pp. 550–591.
- [38] N. PETRA, J. MARTIN, G. STADLER, AND O. GHATTAS, *A computational framework for infinite-dimensional bayesian inverse problems. Part II: Stochastic newton mcmc with application to ice sheet flow inverse problems*, SIAM Journal on Scientific Computing, 36 (2014), pp. A1525–A1555.
- [39] A. K. SAIBABA, J. HART, AND B. VAN BLOEMEN WAANDERS, *Randomized algorithms for generalized singular value decomposition with application to sensitivity analysis*, Numerical Linear Algebra with Applications, (2021).
- [40] A. M. STUART, *Inverse problems: a Bayesian perspective*, Acta Numerica, (2010).
- [41] I. SUNSERI, A. ALEXANDERIAN, J. HART, AND B. VAN BLOEMEN WAANDERS, *Hyper-differential sensitivity analysis for nonlinear bayesian inverse problems*, Submitted. arXiv: <https://arxiv.org/abs/2202.02219>, (2022).
- [42] I. SUNSERI, J. HART, B. VAN BLOEMEN WAANDERS, AND A. ALEXANDERIAN, *Hyper-differential sensitivity analysis for inverse problems constrained by partial differential equations*, Inverse Problems, 36 (2020).
- [43] C. R. VOGEL, *Sparse matrix computations arising in distributed parameter identification*, SIAM J. Matrix Anal. Appl., (1999), pp. 1027–1037.
- [44] C. R. VOGEL, *Computational Methods for Inverse Problems*, SIAM Frontiers in Applied Mathematics Series, 2002.